A BROAD-ANGLE RADOME EMPLOYING REACTIVE WALLS

Alden Gordon Finley

A BROAD-ANGLE RADOME

EMPLOYING

REACTIVE WALLS

* * * *

Alden G. Finley

This work is accepted as fulfilling

the thesis requirements for the degree of

MASTER OF SCIENCE

IN

ENGINEERING ELECTRONICS

from the

United States Naval Postgraduate School

PREFACE

The major portion of the work described in this thesis was accomplished at Stanford Research Institute, Menlo Park, California, during the author's, United States Naval Postgraduate School sponsored, Industrial Experience Tour, 3 January, to 15 March, 1956. The author is indebted to the Postgraduate School and the management of Stanford Research Institute for their cooperative effort in making this opportunity possible. The personal effort and interest of many of the Stanford Research Institute employees is also appreciated. Credit is due in particular to Dr. S. B. Cohn, Head of the Microwave Group, Dr. E. M. T. Jones, and L. A. Robinson for their supervision and guidance; to K. M. Beach, R. W. Remington, N. F. Mangal and B. C. Belt for their valuable technical assistance; and to Miss M. M. Humphrey who performed the greater part of the mathematical calculations.

Acknowledgments are due to Professors C. E. Menneken and J. G. Chaney of the Postgraduate School for their continuous interest in the project and their kind assistance and cooperation in the preparation of this paper. The author is grateful to Mrs. Shirley Kelley for the typing of the finished thesis.

TABLE OF CONTENTS

LIST OF ILLUSTRATIONS

TABLE OF SYMBOLS AND ABBREVIATIONS

B	- Electrical susceptance
B_w	- Electrical susceptance of reactive wall embedded in the radome dielectric
D	- Diameter of the wires in the wire grid
F, F'	- Special correction factors for calculation of the susceptance of the wire grids
f	- Frequency in cycles per second
G	- Electrical conductance
KMC	- Kilomegacycles
n	- Index of refraction of radome dielectric
S	- Center to center wire spacing in the wire grid
t, t', t''	- Radome thicknesses measured in physical units
VSWR	- Voltage standing-wave ratio
Y	- Electrical admittance
Y_c	- Characteristic admittance of special slotted line
Y_{in}	- Input admittance of radome when it is terminated in free space
Y_o	- Characteristic wave admittance of free space
Y_1	- Midplane admittance of radome when it is terminated in free space
Y_2	- Characteristic admittance of radome dielectric
Γ	- Voltage reflection coefficient
δ	- Loss angle
ϵ	- Dielectric constant
ϵ_r	- Relative dielectric constant of the radome dielectric
θ_1	- Angle of incidence as measured in free space

θ_2	- Angle of incidence as measured in radome dielectric
λ_o	- Wavelength as measured in free space
λ_2	- Wavelength as measured in radome dielectric ($\lambda_2 = \lambda_o/n$)
μ	- Permiability
ρ	- Magnitude of the voltage reflection coefficient
ϕ, ϕ', ϕ''	- Radome thicknesses as measured in electrical units
$\parallel$ pol.	- Polarization with the electric field component parallel to the plane of incidence
$\perp$ pol.	- Polarization with the electric field component perpendicular to the plane of incidence
$\triangleq$	- By definition
$\Rightarrow$	- Leads to

CHAPTER I

INTRODUCTION

1. The Radome.

Most radar and microwave installations require protection from the weather or from aerodynamic forces. This protection usually takes the form of a dome-like structure--hence the name radome, from radar-dome. Generally, a radome can be eliminated from most ground and shipboard installations. This can be done by making the radar antenna and mount weather-proof and by piercing the antenna with holes to reduce the effects of the wind. Thus, for the most part, radomes are considered only as necessities for aircraft radars and beacons. The aeronautical engineer visualizes the radome as a preponderous bulge on his otherwise streamlined aircraft and the electronics engineer views the radome as an obstacle in the path of the microwave energy radiating to and from his well designed radar antenna. Radome design discussion, therefore, can generally be divided into mechanical considerations and electrical considerations. It is the latter that is of concern in this paper, although some structural aspects will be mentioned. A very comprehensive discussion of radomes is presented in Part II of "Radar Scanners and Radomes" by Cady, Karelitz and Turner. (1)

The production of a satisfactory radome might appear at first as the simple task of placing any suitable material of a suitable shape around the radar antenna. This is very true, but the difficult undertaking comes in finding the "suitable" material and the "suitable" shape. Materials that appear transparent to microwaves of one frequency may be

quite opaque at another frequency. Only little energy may be reflected from the surface of a radome when microwaves impinge upon it from one angle, but such may not be true for other angles. Radomes that have been designed to remain relatively transparent, i.e. present a good impedance match to free space, for several frequencies are called "broad-band". Those designed to be transparent for many angles of incidence are termed "broad-angle".

The opaqueness of a radome to microwaves may be due to energy actually absorbed in the radome material as well as the division of power by reflections from the surfaces of the radome. One undesirable effect of reflections is the production of standing waves in the radar feed system which tends to detune the microwave source from its proper frequency. This phenomenon is known as "pulling". Dispersion of the radar beam and the phase shift which the microwaves experience in passing through the radome are other undesirable effects. These irregularities manifest themselves in loss of range and distortion of the radar presentation. Very often serious degradation of the radar image is caused by only minor anomalies in the path of the radiation. The search for a "better radome" has been in existance since the conception of airborne radar. The difficulty is often compounded because many of the radome characteristics are not independent and an improvement for one often makes another worse.

2. Types of Radomes.

Radomes may be divided into two broad classes--normal-incidence radomes and streamlined radomes. In the first group there are the flat, cylindrical and spherical radomes upon which, for the most part, the

microwaves from a radar scanner are incident at zero degrees. When the radome deviates so much from one of these shapes that it is no longer possible to consider the microwaves normal to the surface, then it may be called streamlined.

The simplest of designs for a normal-incidence radome is the plain, or isotropic, dielectric sheet. Next to having no radome at all, the best procedure is to have a very thin one. To achieve the desired protection from the elements, a thin radome would not be at all practical, since, to be useful, it would have to be less than .02 wavelengths thick. At X-band this is about .016 inches. For one frequency and one angle of incidence, an isotropic radome can be made a "match" to free space, and thus appear transparent to microwaves by making it an integral multiple of a half-wavelength thick. The reason for this, as in many other half-wavelength devices, is the mutual cancellation of reflections emanating from the front and the rear walls of the radome. Despite its desirable characteristics, there are serious reasons why such a radome may not be used. Its electrical properties are very frequency-sensitive and often, a half-wavelength thick radome is too heavy for practical use.

Cancellation by the same phenomenon as that occurring in the half-wavelength radomes can be obtained by placing two thin sheets an odd multiple of a quarter-wavelength apart. (Unlike the solid radome, where the reflected wave from the far dielectric surface suffers a 180 degree phase reversal--dictating a half-wavelength thickness for cancellation--the reflection from the second thin sheet is in-phase. A quarter-wavelength spacing is necessary, therefore, to produce

cancellation between the two in-phase reflected waves from the two thin sheets.) This type of radome construction is called a double-wall, or "sandwich" radome. It is about half as thick as the half-wave radome, and when the airspace between the two "skins" is filled with a suitable "core" material, the construction is considerably stronger mechanically. Unfortunately, the use of a core material degrades the mutual cancellation effect, and a compromise design must be obtained before suitable sandwich radomes can be fabricated. Despite these complications, this type of radome construction is the most common in use today.

The impedance match to free space required over a wide range of angles in the streamline radome further complicates the problem. The half-wavelength radome for normal incidence is no longer a half-wavelength thick for other angles of incidence, and therefore, no longer transparent. At best, a slightly thicker than a half-wavelength radome is only a compromise. By using sandwiches of various designs, different types of material, and different thicknesses of skins and cores, fairly broad-angle radomes can be designed that are structurally adequate. By a further expedient of varying the thickness of the core within a given radome, a more constant match can be obtained at the various angles of incidence as the radar scanner oscillates. Such a radome may be constructed by the "foamed in place" method. In this process the skins are placed over properly shaped mandrels and the core material is chemically formed between the two skins by foaming it from a liquid state.

In high speed aircraft the shape of the radome becomes more pointed and the structural requirements more rigid. A forward looking radar

scanner protected by a conical radome may be required to do most of its "looking" through a heavy radome at a very high angle of incidence. Materials having a high dielectric constant and otherwise possessing poor electrical characteristics may be required because of their mechanical properties. The type of "loaded" radome design, which is the subject of this thesis, may provide the answer to some of these pressing requirements.

CHAPTER II

REACTIVE WALLS IN RADOME DESIGN

1. "Loaded" Radomes.

In much the same fashion as the term "loading" is used in antenna design, a "loaded" radome may be considered as one that has been modified electrically by the inclusion of a reactive element. This reactive element usually takes the form of an array of wires or metallic discs, either on the surface of the dielectric or embedded in it. By means of analytical calculations, it can be shown that a grid of parallel wires will appear inductive, and that an array of thin metallic discs will appear capacitive to plane electromagnetic waves incident upon them. By use of such arrays--which may be considered as "reactive walls"--the electrical properties of a dielectric sheet may be modified to provide a radome design of unusual characteristics.

An isotropic radome of a half-wavelength thickness, which has been mentioned, has a perfect impedance match to free space at one particular angle of incidence and one particular frequency. For a very narrow range about these values the radome may be considered to have a "good match" to free space, and thus be usable. Indeed, the characteristics vary so greatly with a change of frequency or angle that the usable band is extremely narrow. For the most part, the reactance of a wire grid or array of discs is less dependent upon these variables. By judicious inclusion of such reactive walls in the dielectric, the range of frequency and/or angles of incidence over which the radome is usable may be increased.

2. Stanford Research Institute Project 1115.

Since 1 July, 1954, Stanford Research Institute has been involved in a United States Army contract entitled, "Investigation of Wide-Band Antennas above 2000 MC" (2). One phase of this contract is concerned with wide-band radomes. In an effort to overcome many of the difficulties mentioned in Chapter I, they have directed their attention in this field to the design of radomes employing "reactive walls". They have been able to design radomes which have a desirable electrical match to free space over a wide range of frequencies. The effects of various combinations and placements of these reactive walls have been investigated by analytical methods and several experimental models also have been constructed and tested for their broad-band capabilities.

The main impetus of the project has been directed toward the design of wide-band devices; however, considerable effort has been expended on the consideration of broad-angle radomes as well. Theoretical investigations were reported in November, 1955, (3) on broad-angle radomes which contained a single reactive wall. (Much of the following terminology will not be introduced formally in this paper until Chapter III; however, the chronology of events dictates its inclusion at this time.) This report showed that by use of a single embedded array of parallel wires--which behaves electrically as an inductive reactive wall--it is possible to design a radome to have a match to free space at any angle of incidence for electromagnetic waves polarized perpendicular to the plane of incidence. For waves polarized parallel to the plane of incidence, a single inductive reactive wall will improve the match for angles less than the Brewster angle, but will degrade the performance of the radome

for angles greater than the Brewster angle. A single capacitive reactive wall will perform just oppositely for parallel polarization and will always degrade the match for perpendicular polarization. It is evident that by use of a single reactive wall of either type it is impossible to obtain a good match over the entire range of angles of incidence simultaneously for the two polarizations.

3. Multiple Reactive Walls.

A broad-angle radome cannot be designed which includes only one reactive wall, but it is presumable that a combination of reactive walls of different number, type or placement could provide the desired characteristics. Although no active work was in evidence by January of 1956, on the design of a broad-angle radome employing multiple reactive walls, the possibilities were manifest. Stanford Research Institute was interested in any contribution that could be made in this field, and it was at this research institution that the body of the work, with which this thesis is concerned, was actually accomplished.

Among the problems facing anyone who should have wished to investigate these possibilities were: 1) The selection of the type, number and combination of reactive walls that would lead to the desired results; 2) the origination of a design procedure which would optimize the broad-angle nature of the radome; 3) the design of an actual test sample and the associated fabrication equipment and procedures; and 4) the construction and testing of this test sample in order to validate the theory as well as the optimized design technique. From previous considerations, an investigation of the broad-angle possibilities of a radome loaded with two inductive reactive walls appeared most promising.

4. Introduction to the Remaining Chapters.

In the following chapters, the theory and design of a broad-angle radome using two embedded reactive walls will be considered in detail. In addition to the discussion of the basic equations relating the radome parameters, the step-by-step procedure of an optimized design technique will be presented. The construction and testing of a sample radome will be described and finally the results will be evaluated. It is at this point that the general nature of this paper ceases, and its scope narrows to include solely one type of radome design.

CHAPTER III

THE DESIGN OF A BROAD-ANGLE RADOME USING TWO EMBEDDED REACTIVE WALLS

1. Introduction.

In the design or analysis of radomes, it is very convenient to use equivalent transmission-line circuits. This technique provides exact solutions only for plane electromagnetic waves and radomes of infinite extent. Satisfactory results can be obtained if these conditions are approximated by having the radome area, plus the radii of curvature of the incident wave front and radome surface, large with respect to a wavelength. In practice, most radomes are of a streamlined shape. The behavior of such a curved radome can be simulated for any oblique angle of incidence by visualizing it as many small flat areas; each upon which the electromagnetic wave is incident. It is desirable to have no energy absorbed in the radome material. Besides the actual savings of energy, a simple relation exists between the reflected and transmitted power. For these and other reasons, all of the radome dielectric materials discussed in this paper will be considered lossless.

2. Use of the Smith Transmission-line Chart.

Transmission-line problems can most easily be handled by use of the Smith transmission-line calculator or chart. (4) One can obtain the impedance at any point in the dielectric material of a radome merely by manuvering in the proper manner on such a chart. Since most of the calculations involve the impedance of the dielectric, it is convenient to normalize to the impedance of the dielectric material. It is also convenient to use admittances, since, as it will be shown later, a wire

grid is best represented as a shunt, inductive susceptance. In using the Smith chart, it is not necessary to proceed all the way from a known terminal admittance to the driving point of the radome to obtain information that is needed for design. It is shown in Appendix I that the reflection coefficient, standing wave ratio, power insertion loss, per cent power transmitted, etc., for a symetrical radome can be completely and more easily described from information taken only at the midplane of the radome.

Any movement or value on a Smith chart can be expressed in analytical form. It is advisable in the actual design of a broad-angle radome to use graphical techniques and to use the analytical equations for verification of the final design. The analytical form also can be adapted for solution by a computer, thus enabling the engineer to assemble a family of theoretical curves for different parameters once a suitable design has been established.

3. A Discussion of the Radome Parameters.

A cross-sectional diagram of a radome with two embedded wire grids is shown in Figure 1. With this figure and the Table of Symbols and Abbreviations at hand, it is desirable at this time to discuss the significance of each of these descriptive functions. They will be discussed briefly with defining equations and explanations given where necessary. For a thorough discussion of electromagnetic waves and dielectrics, a volume devoted to this subject should be consulted. (5)

a. Polarization--The "plane of incidence", which is referred to throughout the text, is defined by the normal to the surface on which an electromagnetic wave impinges, and a ray following the direction of

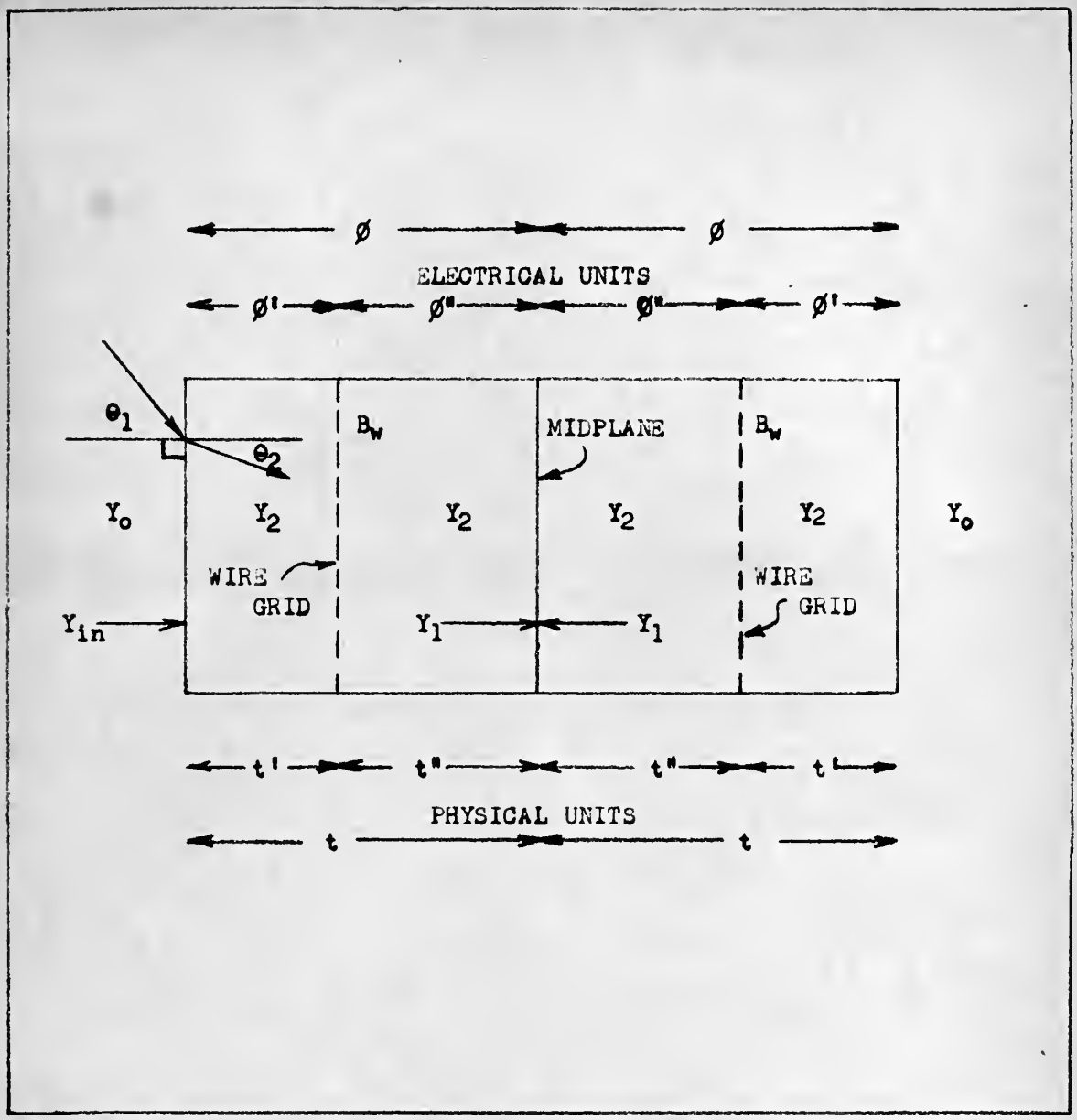

FIG. 1 RADOME CROSS-SECTION WITH PERTINENT PARAMETERS.

propogation of the incident wave. A singly polarized electromagnetic wave incident on a surface, such that its electric field component is perpendicular to the plane of incidence, is referred to as "perpendicularly polarized". In a similar fashion, if the wave is oriented so that its electric field component lies in the plane of incidence, this condition is called "parallel polarization". Since any electromagnetic wave can be resolved into mutually perpendicular components, it is not necessary to consider more than the two polarizations defined.

b. Terminal or load admittance--The load for the actual radome, as well as the transmission-line equivalent, is free space. The characteristic admittance of free space is

$$\sqrt{\frac{\epsilon}{\mu}} \approx \frac{1}{120\pi} \qquad (3\text{-}1)$$

All of the electromagnetic wave calculations in this paper are based on "wave admittance". Wave admittance is defined as the ratio of the magnetic to electric field components in planes parallel to the dielectric surface. A wave at any oblique angle of incidence can be considered as being composed of two perpendicular waves traveling at higher phase velocities such that the composite wavefront progresses without change. This is similar to the use of "phase velocity" in wave guide calculations. Its use is convenient since all oblique angles can be treated like normal incidence because of the continuity of the tangential components at the air-dielectric boundry. The walls of the radome are parallel to each other, thus the angle of incidence in free space is the same for the incident and transmitted waves. The characteristic

wave admittance of free space becomes:

for perpendicular polarization

$$Y_{0_\perp} = \frac{\cos \theta_1}{120\pi} \tag{3-2}$$

and for parallel polarization

$$Y_{0_{||}} = \frac{1}{120\pi \cos \theta_1} \tag{3-3}$$

These values are constant with frequency and are independent of the dielectric material of the radome. They are real functions of θ_1.

c. Characteristic admittance of the dielectric--A lossless dielectric of relative dielectric constant ϵ_r, has a characteristic admittance

$$Y = \frac{\sqrt{\epsilon_r}}{120\pi} \tag{3-4}$$

By definition $\sqrt{\epsilon_r}$ is equal to n, the index of refraction, by which it can be replaced. The wave admittance of the dielectric becomes:

for perpendicular polarization

$$Y_{2_\perp} = \frac{n \cos \theta_2}{120\pi} \tag{3-5}$$

and for parallel polarization

$$Y_{2_{||}} = \frac{n}{120\pi \cos \theta_2} \tag{3-6}$$

These values are constant with frequency, but do depend upon the characteristics of the dielectric and the angle of the wave in that medium. They are real functions when the dielectric is lossless.

By Snells Law (6) θ_2 can be expressed in terms of θ_1.

$$n \cos \theta_2 = \sqrt{n^2 - \sin^2 \theta_1} \tag{3-7}$$

Y_2 then can be expressed as a function of θ_1 and the index of refraction of the dielectric:

for perpendicular polarization

$$Y_{2\perp} = \frac{\sqrt{n^2 - \sin^2 \theta_1}}{120\pi} \tag{3-8}$$

and for parallel polarization

$$Y_{2\parallel} = \frac{n^2}{120\pi\sqrt{n^2 - \sin^2 \theta_1}} \tag{3-9}$$

d. Inductive susceptance of the wire grid--A complete discussion of this topic is beyond the scope of this paper. (2) The susceptance of a wire grid with the wires oriented parallel to the electric field, but with the electric field perpendicular to the plane of incidence has been computed by MacFarlane. (7) It is

$$B_{W\perp} = \frac{-\lambda_2 Y_2}{S \cos \theta_2} \left[\frac{1}{\log_e \left(\frac{S}{\pi D} \right) + F'} \right] \tag{3-10}$$

The inductive susceptance of a wire grid with the wires again oriented parallel to the electric field, but with the electric field parallel to the plane of incidence, can be obtained by applying Babinet's transformation (8) to the solution for the capacitive strip given by Marcuvitz. (9) The resulting equation is

$$B_{W_{\parallel}} = \frac{-\lambda_2 Y_2}{S \cos\theta_2} \left[\frac{1}{\log_e \left(\csc \frac{\pi D}{S} \right) + F} \right] \qquad (3\text{-}11)$$

The correction factor F and F', both functions of θ_2 and S/λ_2, when $D \ll S$, are plotted in Figure 2.

B_w is the reactive component of an admittance of which G, the real part, is zero. Therefore, it must be used as a pure imaginary. It is negative because inductive susceptance is negative. The values of B_w are functions of the wire size and spacing, frequency, index of refraction of the dielectric and to a lesser extent, the angle of incidence. Although the above equations are based on theoretical considerations, experimental verification (2) has shown that they may be employed with very little loss of accuracy for samples of finite dimensions.

e. Input admittance--Although functions of its value are desired, an explicit solution for the input or driving point admittance, Y_{in}, is not needed. As shown in Appendices I and II, the desired information about the behavior of the radome can be obtained solely from a knowledge of the midplane admittance, Y_1. Even this is not needed in explicit form.

f. Midplane admittance--This, as the name implies, is the input admittance as seen from the midplane of the radome when it is terminated

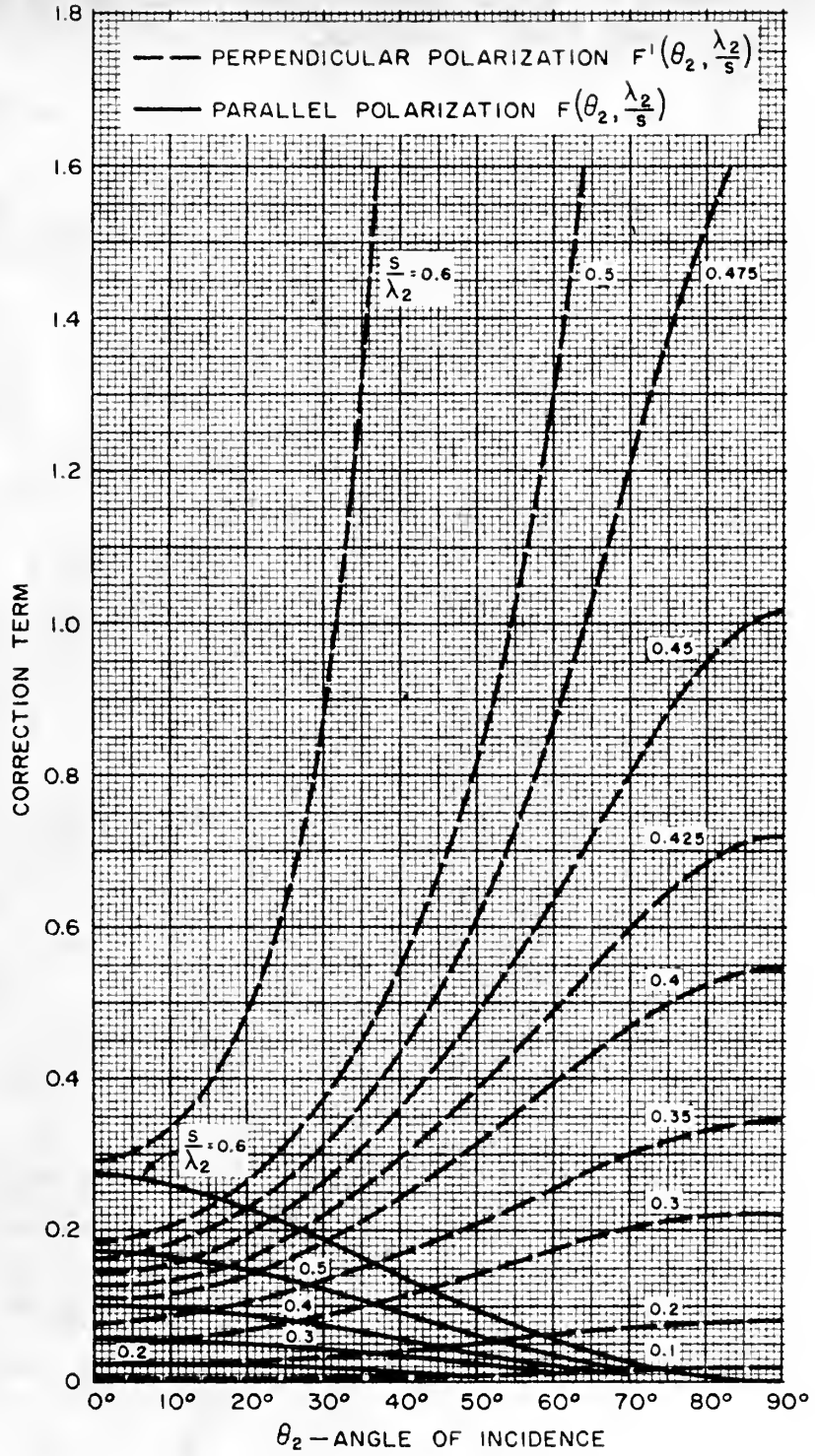

FIG 2 CORRECTION FACTORS FOR REACTANCE OF INDUCTIVE GRIDS.

in free space. A plot of the locus of this admittance on a Smith chart for the two polarizations and various angles of incidence is the most important single tool in the design procedure. If the midplane admittance is a pure conductance (for a lossless, symetrical network with a pure conductance termination), then it should be obvious that Y_{in} will equal the load admittance and no reflections will exist. For a more rigorous proof of this procedure, see Appendix I.

g. Radome thickness--It is advantageous to refer to the thickness of the radome in both electrical units and physical units. The radome is measured in physical units with a micrometer or scale. The electrical thickness of the radome is measured in the wavelengths or degrees of phase shift for a nonreflected wave passing through the dielectric. The equation for electrical thickness expressed in wavelengths is

$$\phi = \frac{t}{\lambda_2} \cos \theta_2 \qquad (3\text{-}12)$$

It is a function of frequency, the properties of the dielectric and the angle of incidence. It is, however, independent of the polarization of the incident energy.

4. Introduction to Graphical Design Procedure.

As noted above, the most important design tool is the locus of Y_1/Y_2, the normalized midplane admittance, on the Smith chart. The procedure for establishing such a plot will now be introduced. With the aid of Figure 3, one can proceed for each angle of incidence, usually every 10 or 20 degrees, and for the two polarizations at the design frequency, step by step as follows:

FIG. 3

ILLUSTRATION OF GRAPHICAL DESIGN TECHNIQUES.

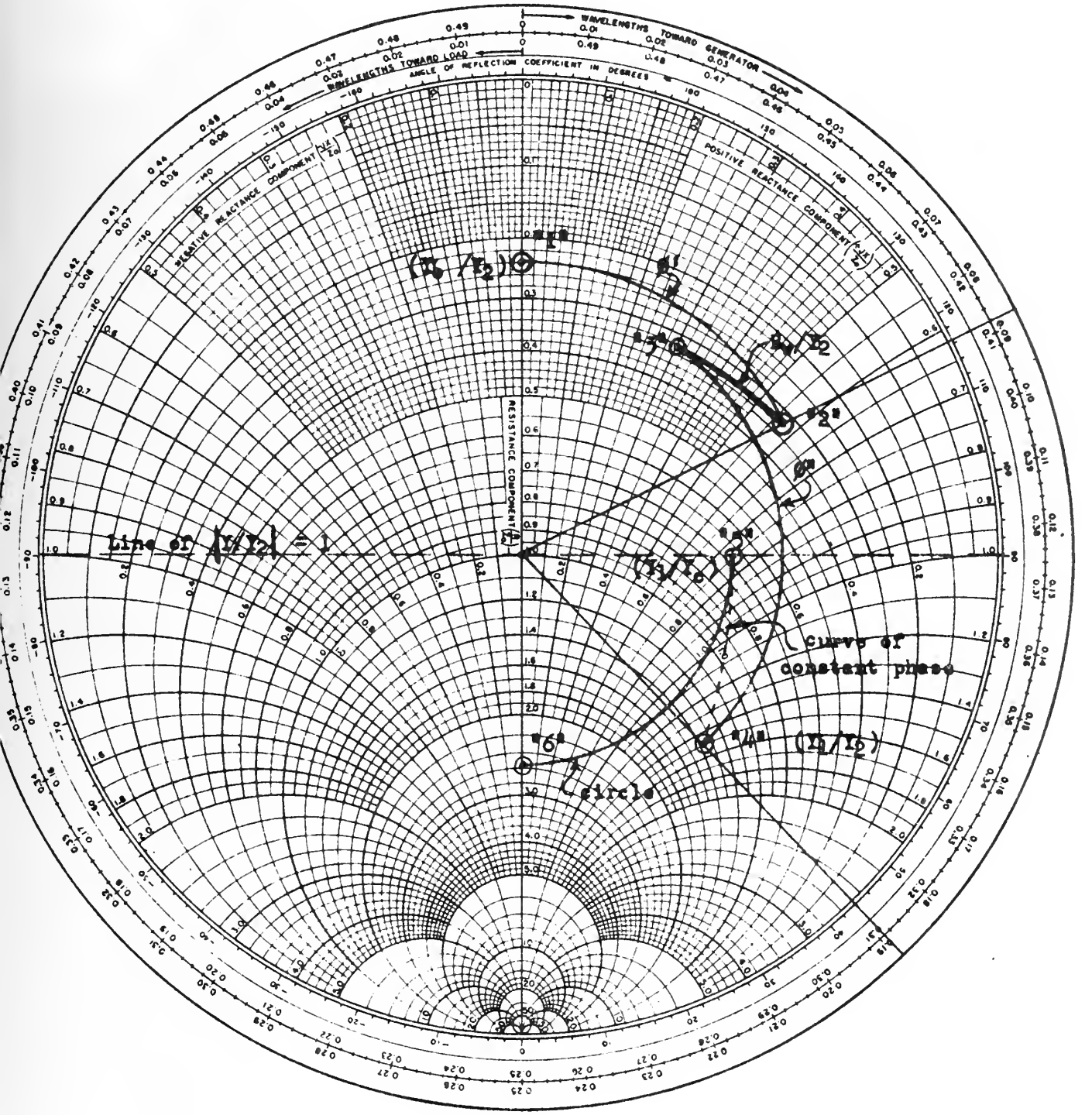

a. Point "1", Y_o/Y_2--The normalized terminal admittance is first computed and plotted on the chart. From equations (3-2) and (3-8), as well as (3-3) and (3-9), one obtains:

for perpendicular polarization

$$Y_o/Y_{2\perp} = \frac{\cos\theta_1}{\sqrt{n^2 - \sin^2\theta_1}} \tag{3-13}$$

and for parallel polarization

$$Y_o/Y_{2\parallel} = \frac{\sqrt{n^2 - \sin^2\theta_1}}{n^2 \cos\theta_1} \tag{3-14}$$

Since these values are real, they will be plotted on the straight line corresponding to the reactive component equal to zero. Note that for θ_1 equal to zero, Y_o/Y_2 is the same for both polarizations. This is true in general for the other parameters also.

b. First thickness of dielectric--From point "1", one proceeds in the direction toward the generator, on a constant attenuation circle, the electrical thickness of the first layer of dielectric. Thus point "2" is the normalized admittance looking toward the load from a point just on the load side of the wire grid.

c. The susceptance of the wire grid--From point "2", one must add the negative susceptance of the wire grid as calculated from equations (3-10) and (3-11). One proceeds in a negative reactance direction the distance equivalent to the value of B_w/Y_2. Point "3" is then the normalized admittance looking toward the load from a point that just includes the wire structure.

d. Half of the middle thickness of the dielectric--From point "3", one proceeds in the direction toward the generator one half of the electrical thickness of the middle section of the dielectric to point "4". This is the desired normalized midplane admittance.

Repeat this procedure at the design frequency for the several angles of incidence and the two polarizations. A line drawn through the resulting point "4"'s is the locus required for design. A typical locus is shown in Figure 4.

It will be shown that by use of this plot, the thicknesses of the dielectric and the size and spacing of the wires in the wire grid can be manipulated with a good knowledge of which way they should be changed to obtain the desired results. A plot of Y_1/Y_2 for a perfectly transparent radome would be a straight line on the conductance component axis of the Smith chart. The closer the actual locus comes to this real axis, the better is the broad-angle properties of the radome.

5. Determination of Initial Values.

A logical question at this point might well be, "What values of $\emptyset'$, $\emptyset''$, S, D, and the other parameters are chosen to start with?" In answer to this question, several reasonably obvious comments can be made before more precise procedures are discussed. A broad-angle radome is often a narrow-band device. For this reason a particular design frequency should be chosen at which the radar equipment is intended to operate. The physical thickness of the radome as well as the material of which it is made should be commensurate with its mechanical requirements. The diameter and spacing of the wires should be chosen within the realm of physical realizability. A wire of .001 inch diameter is

FIG. 4

MIDPLANE ADMITTANCE DIAGRAM FOR ILLUSTRATIVE LOADED RADOME DESIGN.

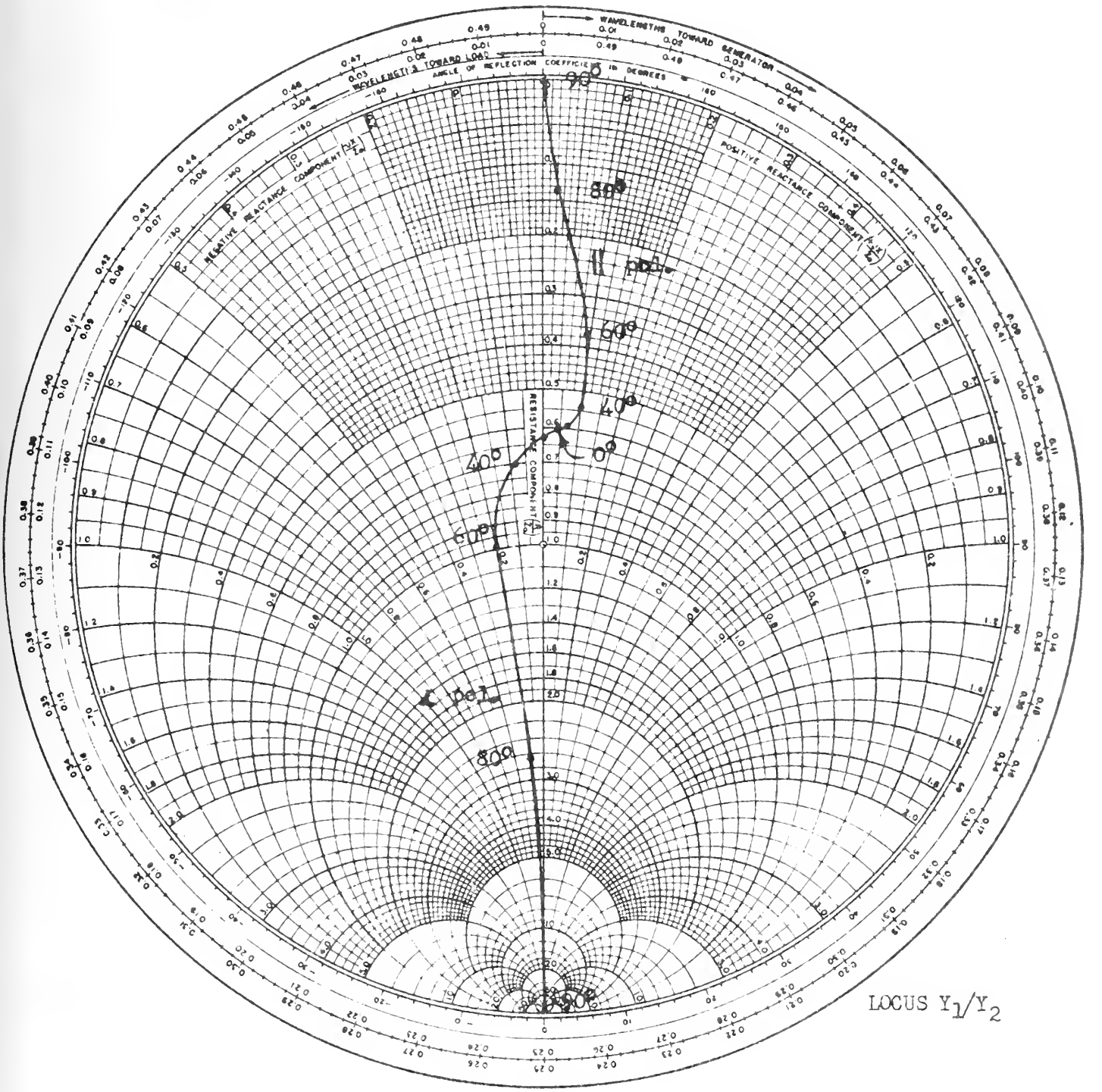

difficult to work with. And it is ridiculous to attempt to make a grid with wire of a diameter greater than its spacing. On the other hand, the spacing should not be so great as to cause multiple scattering, i.e. planes of constant phase existing from angles other than the angle of reflection. To this end, the following inequality should be maintained

$$\frac{s}{\lambda_2} \leq \frac{1}{1 + |\sin \theta_2|} \qquad (3\text{-}15)$$

6. Midplane Technique used for an Isotropic Radome.

In establishing values for a loaded radome design by the midplane admittance technique, it might be well to consider the design of an isotropic radome by this method. As discussed in Chapter I, a radome that is a half-wavelength thick and lossless is a match to free space. However, since the electrical thickness of a dielectric is a function of frequency and the angle of incidence (see equation 3-12), this half-wavelength thickness cannot be met except at discrete frequencies and angles of incidence. At a particular design frequency the physical thickness of an isotropic radome can be chosen so that its electrical thickness is a half-wavelength, and therefore, a match to free space only at a particular angle of incidence. (There will also be a match at the Brewster angle for parallel polarization.)

This fact can be demonstrated on the Smith chart by the midplane admittance locus. The real values of normalized terminal admittance for each angle of incidence are rotated through the electrical half-thickness for that particular angle. When the electrical half-thickness is a quarter of a wavelength, the plot of Y_1/Y_2 will be on the real

axis of the Smith chart. This corresponds to a perfect match. The plot of Y_1/Y_2 for the other angles of incidence will lie elsewhere on the chart--indicating mismatches.

In determining the physical thickness necessary to give a match at a particular angle of incidence, it is necessary to solve equation (3-12) for t when $\emptyset$ equals a half wavelength. Equation (3-12) can be written in a more desirable form, which shows $\emptyset$ as a function of λ_o and θ_1, by applying Snell's Law,

$$\emptyset = \frac{t}{\lambda_o}\sqrt{n^2 - \sin^2\theta_1} \qquad (3\text{-}16)$$

When $\emptyset$ is set equal to 1/2, the physical thickness required for a match at θ_1 becomes

$$t = \frac{\lambda_o}{2\sqrt{n^2 - \sin^2\theta_1}} \qquad (3\text{-}17)$$

In designing an isotropic radome which is to have broad-angle transmission efficiency, there is very little that can be done to make the locus of Y_1/Y_2 coincide with the real axis of the Smith chart for all angles of incidence. In Appendix I it is shown that the reflection increases the further the locus of Y_1/Y_2 is from such coincidence. Although physical reasoning would indicate that a perfect match at $\theta_1 = 90^\circ$ is impossible, nevertheless, a <u>design</u> for such an occurrence will yield a radome that has the broadest angle transmission. A mid-plane admittance diagram for such a design is shown in Figure 5. This

FIG. 5

MIDPLANE ADMITTANCE DIAGRAM FOR AN ISOTROPIC RADOME DESIGNED FOR A MATCH AT 90°.

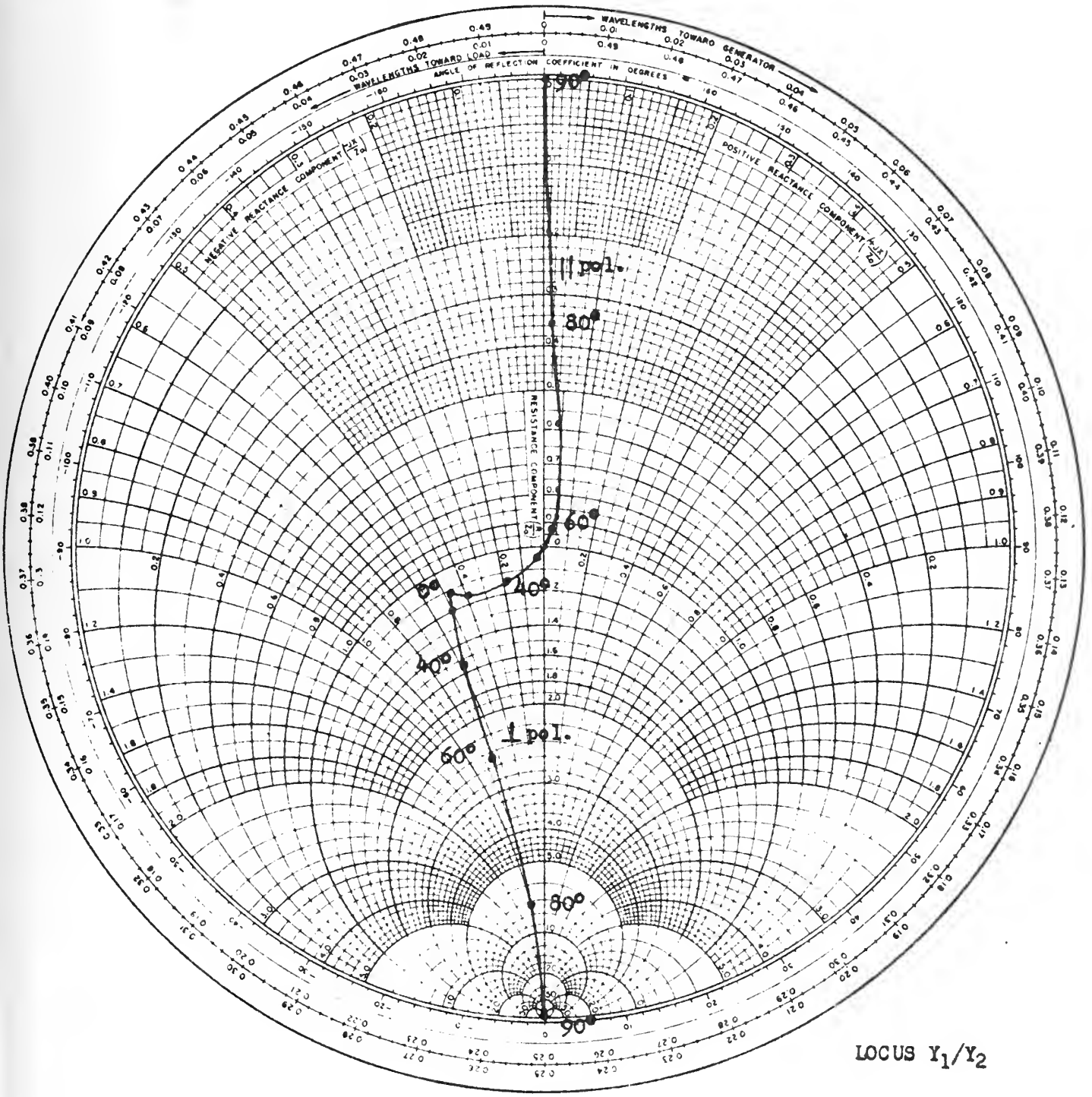

LOCUS Y_1/Y_2

reasoning becomes evident when one attempts to match at any other angle of incidence. Although the reflection peak at normal incidence can be decreased, the reflection at the higher angles will increase surprisingly. (If a good response is desired over only a portion of the possible angles of θ_1, then a better match can be obtained, generally, by considering that particular range of angles.) It is doubtful that one would find use for such a technique in the practical design of isotropic radomes. It will, however, be shown that this "90° angle matching technique" can be used to advantage in determining the values of the many variables present in a loaded radome design.

7. The "90° Angle Matching Technique" in Loaded Radome Design.

One method of visualizing the effect of the wire grids is to consider the midplane admittance diagram -- just described -- for an isotropic radome designed for a match at θ_1 equal to 90°. A discrete addition of a negative susceptance will so skew this locus of Y_1/Y_2 that the large peak at $\theta_1 = 0$ can be reduced. It is necessary, in adding this negative susceptance, that care is taken not to increase the reflection at the larger angles. Since $\emptyset$ is independent of polarization, but B_w/Y_2 is not, any addition of a negative susceptance must be balanced for both polarizations in order to achieve the broad-angle response desired. $\emptyset$ and B_w/Y_2 are measured identically only on the circumference of the Smith chart where $\theta_1 = 90°$. This property can be appropriately combined with the fact that a $\theta_1 = 90°$ match design will yield a very broad-angle radome.

An illustrative example will show how this may be accomplished. Suppose that, by reasons based upon physical requirements, a trial set

of wire spacing and diameter yields the following values of normalized susceptance:

for perpendicular polarization

$$B_w/Y_{2\perp} = -.467 \tag{3-18}$$

and for parallel polarization

$$B_w/Y_{2\parallel} = -.745 \tag{3-19}$$

What values of ϕ' and ϕ'' should be chosen to assure a match at $\theta_1 = 90^\circ$, and thus assure a broad-angle response? Figure 6 shows how a proper selection of ϕ' and ϕ'' allows the angle subtended by B_w/Y_2, for both polarizations, to be equal. The resulting plot of Y_1/Y_2 is a match at $\theta_1 = 90^\circ$ for both polarizations also. The actual selection of the proper electrical thicknesses for this match can be made either by trial and error or by the solution of a pair of simultaneous equations. These equations are based upon the geometry of the Smith chart. Solutions for ϕ' and ϕ'' can be obtained with little effort.

$$\begin{cases} \tan 2\pi\phi'_{90^\circ} - \left|\dfrac{B_w}{Y_2}\right|_{90^\circ\perp} = \cot 2\pi\phi''_{90^\circ} \\ \cot 2\pi\phi'_{90^\circ} + \left|\dfrac{B_w}{Y_2}\right|_{90^\circ\parallel} = \tan 2\pi\phi''_{90^\circ} \end{cases} \tag{3-20}$$

FIG. 6

ILLUSTRATION OF DESIGN PROCEDURE FOR 90° MATCH ASSURANCE.

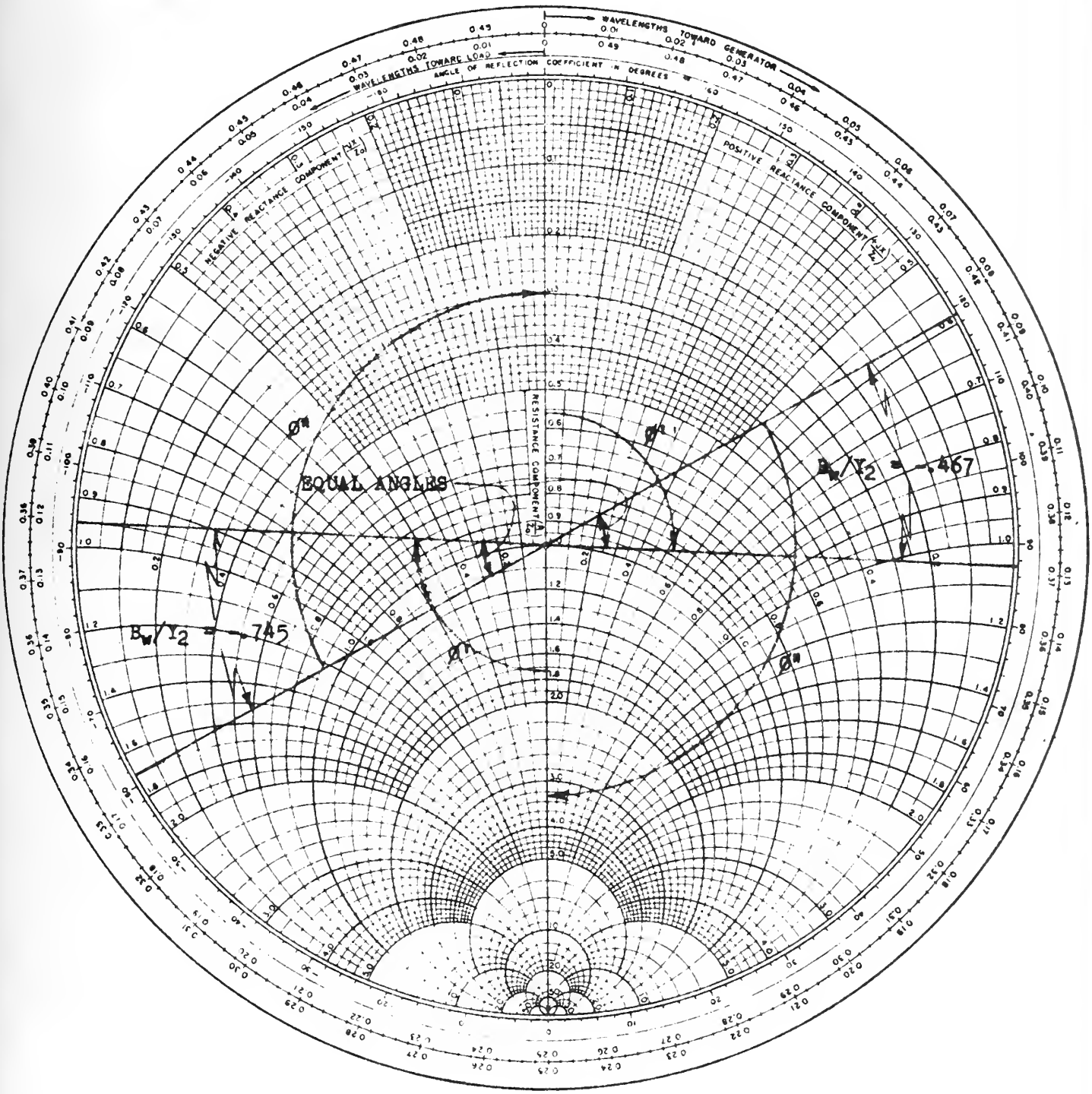

In general, B_w/Y_2 will be almost the same for both polarizations -- the only differences occurring in the values of the correction factors, F and F'. This method thus provides workable values of $\emptyset'$ and $\emptyset''$ for any wire grid susceptance. A larger value of susceptance or smaller value, as indicated by the midplane admittance diagram, should next be tried -- with appropriate values of electrical thickness -- until a locus of Y_1/Y_2 is obtained that is satisfactory. Other methods of determining the parameters may provide broad-angle designs, but this method of 90° match assurance is quite simple and works well.

CHAPTER IV

AN ILLUSTRATIVE EXAMPLE

1. Introduction.

In order to illustrate the theory presented in the previous chapter, the actual design and testing of a sample radome with two embedded reactive walls will be described. The design is presented in a step-by-step manner with each parameter tabulated as its numerical value is developed. It is possible, by substituting other numbers, for one to follow the procedure presented here and obtain a broad-angle design of his own. The construction and testing of the sample radome are discussed briefly and a comparison of theoretical predictions and experimental results is included.

2. Choice of Materials and Dimensions.

The choice of materials used in the construction of the test sample was based on several considerations. The desire to see the adequacy of the bond around the wires of the grids, dictated the use of an optically transparent dielectric. Furthermore, a material of low electrical loss had to be used since the design itself was based on a lossless dielectric. Although polystyrene does not have as high a dielectric constant as the materials commonly employed in radome manufacture. (ϵ_r = 2.5 for polystyrene; ϵ_r = 4 to 9 for fibre glass), it appeared ideally suited otherwise.

Initial calculations indicated that a very fine wire size would be needed for the wire grids. By experimentation, it was found that a #36 wire--.005 inches in diameter--was the smallest size that could be

handled easily in the construction. Beryllium copper, which has a high tensile strength yet low electrical loss, was obtained for this purpose.

A large size radome sample was desired for the tests, especially at high angles of incidence, because the projected area of the sample decreases in proportion to the cosine of the angle of incidence, which is measured from the radome normal. The finished size--18 inches square--was a compromise between the largest dimension that could be accommodated in the bonding and machining equipment, and the smallest area that could be tolerated in the testing procedure.

A design frequency of 9 KMC was chosen in the middle of the 8.5 to 12 KMC frequency band (X-band) on the basis of the availability of test equipment.

3. Design of the Test Sample.

The initial step in the design of the radome test sample was the selection of an operating frequency and a dielectric material.

Operating frequency	f	9.000 KMC
Dielectric material		polystyrene

A table of the characteristics of dielectric materials (10) provided the

Dielectric constant	ϵ_r	2.53

By substitution in the following basic equations:

$$\lambda_o = c/f \qquad (4\text{-}1)$$

$$n = \sqrt{\epsilon_r} \qquad (4\text{-}2)$$

$$\lambda_2 = \lambda_o/n \qquad (4\text{-}3)$$

several more of the numerical values of the invariant parameters were obtained.

Free space wavelength	λ_o	1.3114 inches
Refractive index	n	1.59
Wavelength in the dielectric	λ_2	.825 inches

It was then possible to calculate Y_o/Y_2, from equations (3-13) and (3-14), for the two polarizations and for $\theta_1 = 0^\circ$, 20°, 40°, 60°, 80° and 90°. These points were plotted on the real axis of a Smith chart and labeled for future use.

A plot of the midplane admittance of an unloaded radome of the same material and at the same frequency was desired. This would provide a basis for comparison to illustrate the superior characteristics of the radome with the embedded reactive walls. This plot was obtained by the method described in Chapter III, paragraph 6. With $\theta_1 = 90^\circ$, equation (3-17) was solved.

Physical thickness of isotropic radome	t	$.314\lambda_o$

Substitution of this value into equation (3-16) yielded

Electrical thickness of isotropic radome	ϕ	tabulated as a function of θ_1

From the plot of Y_o/Y_2, which was invariant for a fixed frequency and dielectric constant, the values of $\phi/2$ were added. This was done by rotating in a toward-the-generator direction on constant attenuation circles. It was necessary to divide the values of ϕ, tabulated above, by two because it was the midplane admittance that was desired. The locus of these terminal points was indeed the midplane admittance of

the isotropic radome. This diagram represented the radome that was to be improved by the addition of the wire grids!

From experience, an initial "guess" was ventured as to the amount of susceptance needed to bring this locus into close coincidence with the real axis of the Smith chart and thereby provide the broadest angle design possible. Several tries were made before a suitable value was obtained. (Although the "90° matching technique" guarantees that each design will be optimum broad-angle, it does not provide an optimum set of grid susceptance values.) Only the final calculations will be presented here, since each of the previous computations was accomplished in a similar manner.

A grid of wires with following specifications

Wire diameter	D	.005 inches
Center to center spacing	S	.320 inches

was checked by equation (3-15) for multiple scattering and found to be satisfactory. The inductive susceptance of this wire grid was determined from equations (3-10) and (3-11).

Inductive susceptance of wire grid	B_w	tabulated as a function of θ_1 and the polarization

The values of B_w for $\theta_1 = 90^{\circ}$, for both polarizations, were substituted into equation (3-20) and the values of ϕ' and ϕ'' for $\theta_1 = 90^{\circ}$ were obtained.

Electrical thicknesses of dielectric for $\theta_1 = 90^{\circ}$	$\phi'_{90^{\circ}}$	.162 wavelengths
	$\phi''_{90^{\circ}}$	.166 wavelengths

These values, plus those of B_w for $\theta_1 = 90^{\circ}$, were checked on the Smith chart and were found to be satisfactory. (See explanation in Chapter III,

paragraph 7; and Figure 6.) Then they were substituted into equation (3-16) with $\theta_1 = 90^\circ$ to obtain

Physical thicknesses of dielectric	t'	.172 inches
	t"	.176 inches

All of the values of ϕ' and ϕ'' were next obtained from equation (3-16)

Electrical thickness of dielectric	ϕ', ϕ''	tabulated as functions of θ_1

This completed the calculation of the radome parameters.

As described in Chapter III, paragraph 4, the graphical plot of the midplane admittance was constructed. See Figure 4. By means of a Carter chart overlay (see Appendix I) the values of VSWR were obtained from this plot.

Voltage standing wave ratio of entire radome	VSWR	tabulated as a function of θ_1

From this tabulation any one of a number of descriptive functions could be calculated. The most useful, since it would be obtained directly in the testing procedure, was the voltage reflection coefficient. The conversion equation is

$$\rho = \frac{VSWR - 1}{VSWR + 1} \qquad (4\text{-}4)$$

A plot of ρ versus θ_1 can be seen in Figure 7.

Also useful, since it is a description more easily understood, was the plot of per cent power transmitted through the radome -- Figure 8. The values were determined from the relation

$$\text{per cent power transmitted} = (1-\rho^2)\ 100 \qquad (4\text{-}5)$$

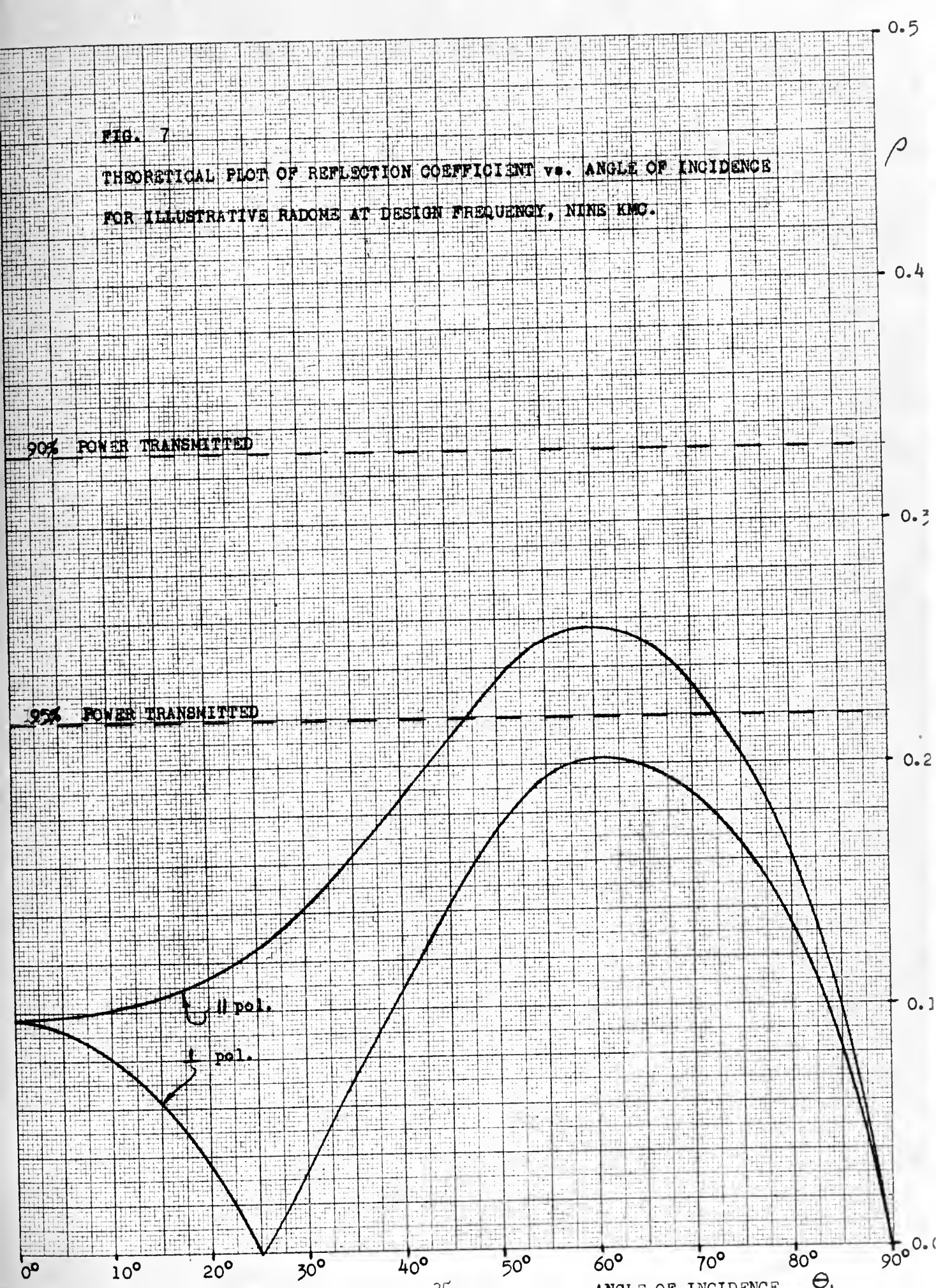
FIG. 7
THEORETICAL PLOT OF REFLECTION COEFFICIENT vs. ANGLE OF INCIDENCE
FOR ILLUSTRATIVE RADOME AT DESIGN FREQUENCY, NINE KMC.
ρ
0.5
0.4
0.3
0.2
0.1
0.0
90% POWER TRANSMITTED
95% POWER TRANSMITTED
|| pol.
⊥ pol.
0°
10°
20°
30°
40°
50°
60°
70°
80°
90°
ANGLE OF INCIDENCE , θ

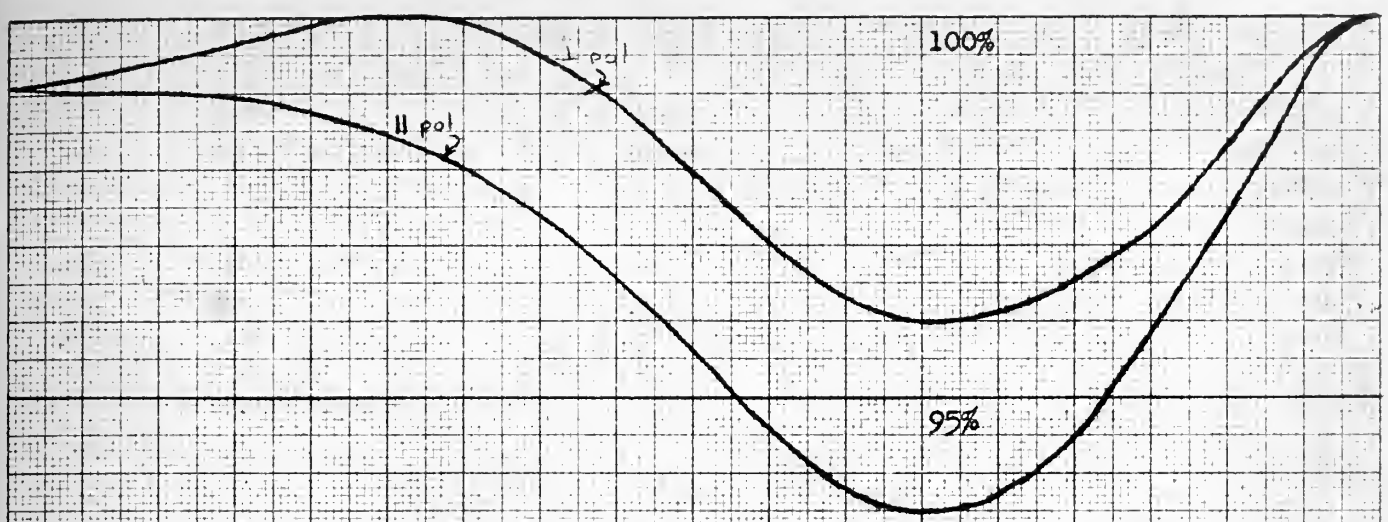

FIG. 8

THEORETICAL PLOT OF PERCENT POWER TRANSMITTED vs. ANGLE OF INCIDENCE FOR ILLUSTRATIVE RADOME AT DESIGN FREQUENCY, NINE KMC.

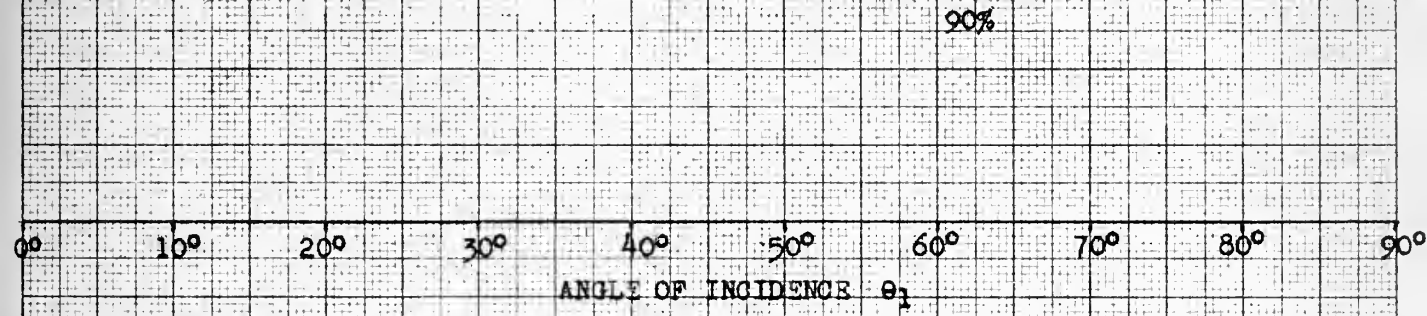

These graphical means were used to establish the initial design and while the radome test sample was being constructed, analytical equations were solved and plotted for a verification and accuracy check. The curves predicted by the analytical equations and by the graphical procedure were similar enough to show that the added calculations were unnecessary.

4. Construction of the Test Sample.

An array of parallel, beryllium copper wires, .005 inches in diameter and spaced .320 inches center to center, were strung from accurately positioned pins on a 20 inch square, steel frame. This array was then sandwiched between two 18 inch square sheets of quarter-inch thick polystyrene plastic. A bonding material, consisting of polystyrene dissolved in styrene monomer, was used about the wires so that the solidified junction would have the same dielectric constant as the sheets of polystyrene themselves. Two such assemblies were made and then accurately machined to the proper thicknesses. Great care was exercised in the machining process to insure the correct placement of the wire grids in relation to the dielectric surfaces. The two finished assemblies were placed back to back, with the wire grids parallel to each other but staggered half of the center-to-center wire spacing. The resulting sandwich was then bound with tape around the edge. To preserve the continuity of the dielectric at the interface of the two assemblies, as well as maintain the designed radome thickness -- by insuring a positive contact along this plane -- a vacuum was applied at this point throughout the entire testing procedure. (For this particular method of construction, no thickness of bonding material could be tolerated between

the two assemblies, since it would render impossible accurate measurement of the inter-grid spacing.) A photograph of a portion of the completed test sample, with the binding tape removed, is shown in Figure 9.

5. Experimental Equipment and Testing Procedure.

The transmission efficiency of the radome was so high that measurement of reflected energy provided a much more accurate method of evaluating the radome than did measurement of the transmitted energy. Figure 10 is a block diagram of the test equipment employed. Two paths were provided between the klystron signal source and the detector--one through free space, via the movable horns and radome, as shown in Figure 11; the other path through a cancellation channel, in which the signal could be varied in phase and amplitude. The equipment was very similar to that used by Redheffer (11). Figure 12 is a photograph of the signal source and cancellation network. A low noise level was achieved in the detector circuit by using a very narrow-band amplifier following the crystal termination. To prevent the klystron modulation frequency from drifting outside of this narrow band (three cycles, flat response, at 1000 cps), synchronization was maintained by the precision tuning fork oscillator.

To reduce stray reflections, a microwave absorbing material was placed behind the test sample and on the upright portions of the horn mounts. The radome sample was held in place before the horns in a low loss, low dielectric constant ($\tan \delta = .0001$, $\epsilon_r = 1.03$), Styrofoam mount, fastened to a sliding platform.

With nothing in front of the horns except the absorbing material,

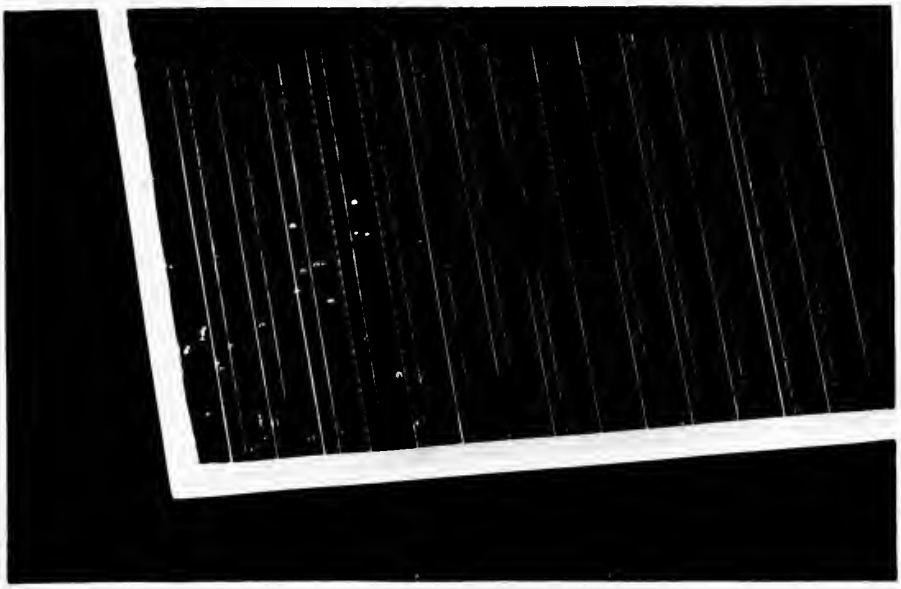

FIG. 9 A PORTION OF THE RADOME TEST SAMPLE.

FIG. 10 BLOCK DIAGRAM OF MICROWAVE EQUIPMENT

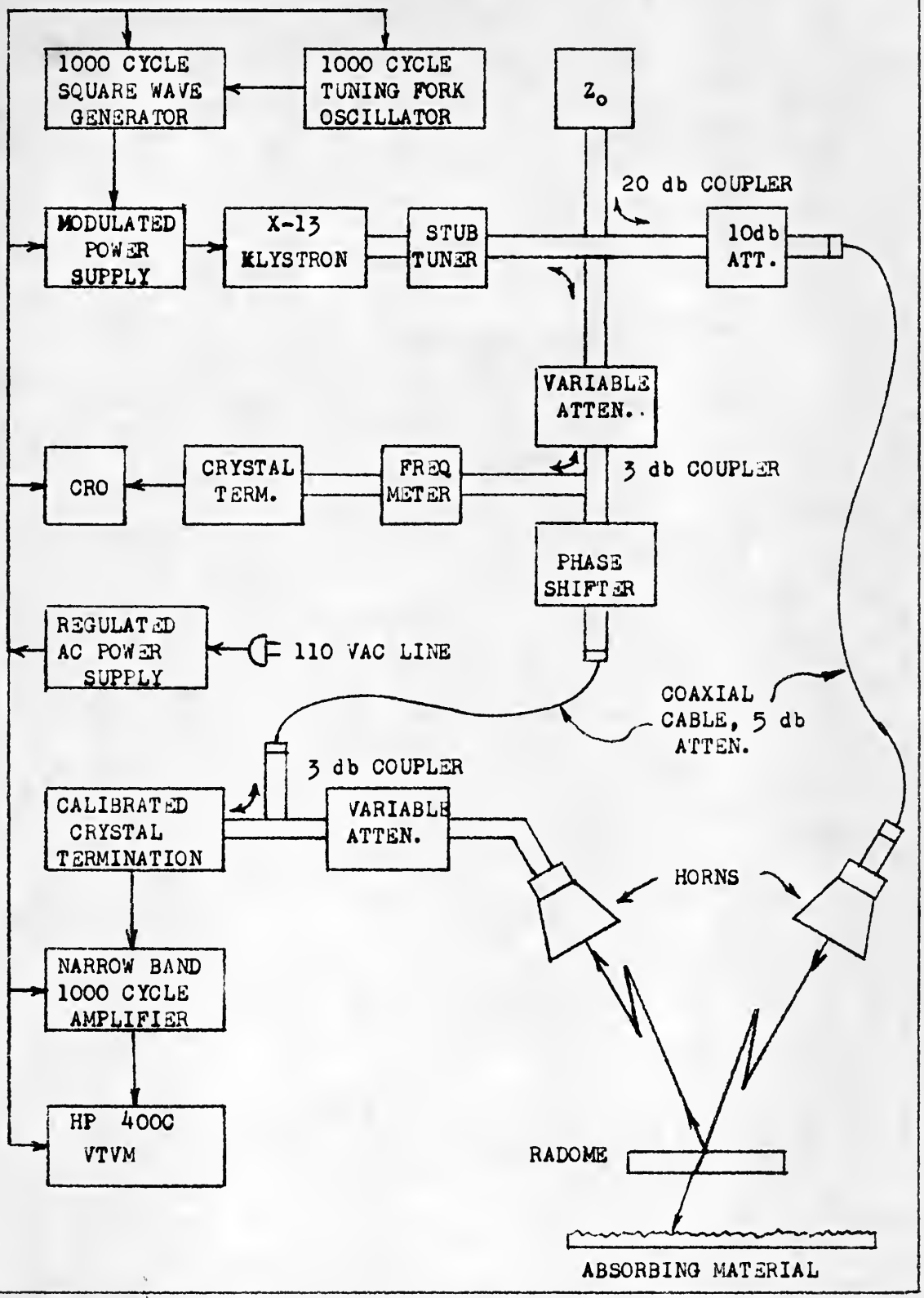

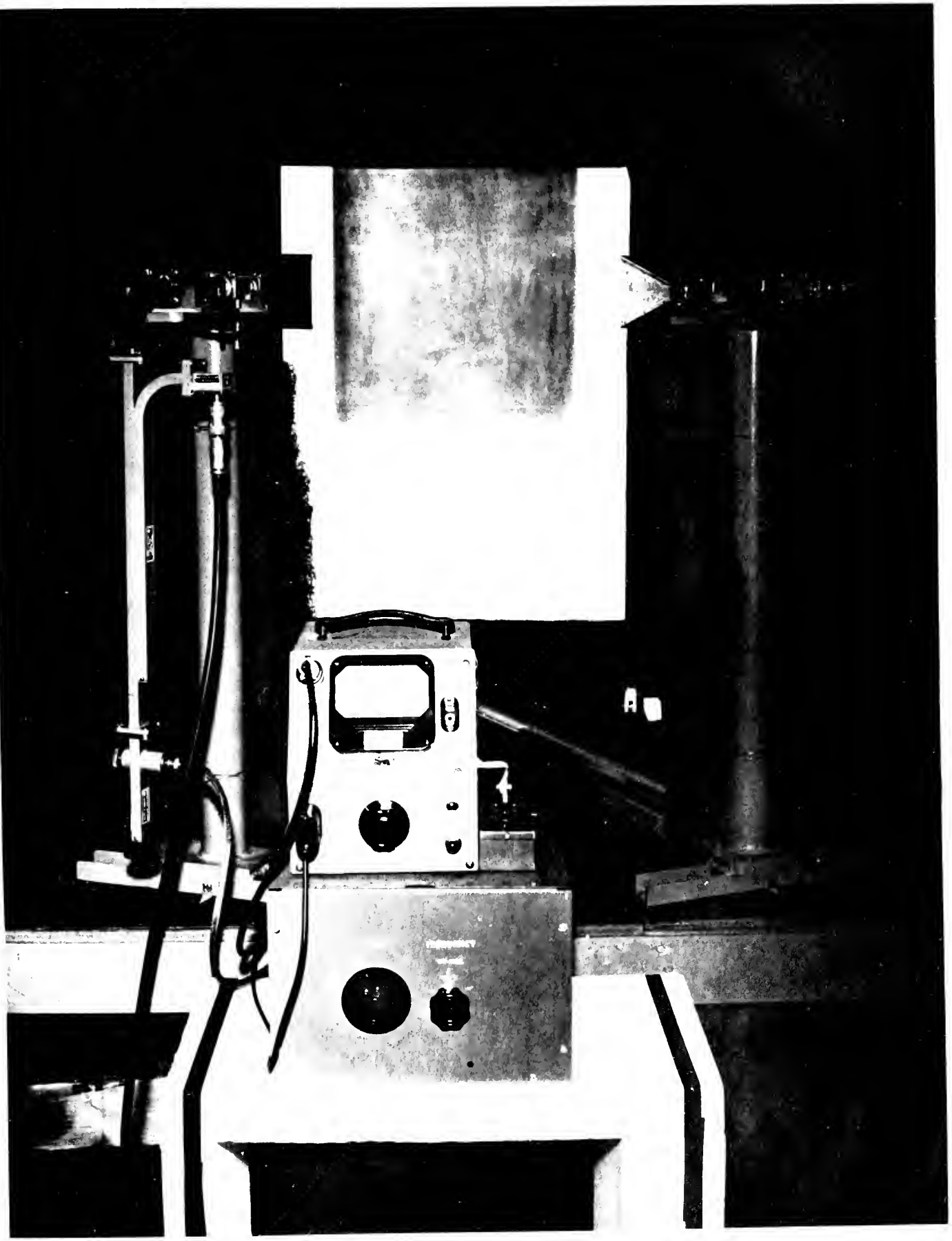

FIG. 11 RADOME [illegible] AND KOMO IN POSITION FOR REFLECTION TESTS.

FIG. 12 MICROWAVE EQUIPMENT [illegible]

the cancellation channel was adjusted to produce a signal, at the crystal termination, of equal magnitude, but opposite phase, to the stray energy coupled through the receiving horn. This condition of zero net signal was indicated by a minimum reading on the vacuum tube voltmeter. The test radome sample, mounted in the Styrofoam mount, was then placed at the intersection of the axes of the two horns, which had been adjusted to form equal angles at the surface of the radome. Because of the square-law characteristics of the crystal, the power level of the reflected energy was observed directly on the voltmeter. The movement of the test sample on a sliding platform, along the direction of the radome normal, provided sufficient readings so that the effects of standing waves, caused by multiple reflections and diffraction, could be averaged. The average power level of the reflected energy from a "standard" of equal area -- the reflection coefficient of which was known--mounted in an identical Styrofoam mount, and in the same physical position as the test radome, was next recorded. From a comparison of these two readings, the reflection coefficient of the radome test sample was calculated.

By moving the horns about on a circle, at the center of which was located, alternately, the test radome and the standard, comparative readings were made for all the angles of incidence from 10° to 70°. A 90° rotation of the radome and the horns in their respective mounts allowed measurements to be made at either polarization. No measurements were made at normal incidence since they were not considered necessary.

6. Evaluation of Experimental Results.

The curves of voltage reflection coefficient versus angle of

incidence for RADOME A and RADOME B are presented in Figures 13 and 14. RADOME A is the double wall loaded radome test sample actually constructed. Two curves are shown for this radome in each figure; one is predicted from theory, and the other is that measured by experiment. RADOME B is a theoretical isotropic radome designed to be broad-angle by making it a match to free space at an angle of incidence of 90°. It is the same isotropic radome discussed previously.

Comparing RADOME A and RADOME B, it can be seen that for parallel polarization, the reflection from the isotropic radome is less than that from the double inductive wall radome, over a small range of angles of incidence. It is obvious, however, when the entire range of angles and both polarizations are considered, that the loaded radome is superior.

The two curves for RADOME A -- theory and experiment -- deviate somewhat from one another. It is difficult to conceive that either the testing procedure or construction was of sufficient accuracy to insure absolute agreement between the two curves. Furthermore, there are some factors that have been neglected in the theory and design that are not completely negligible in the tests. Suffice it to say, that the radome test sample does possess extremely broad-angle properties at the design frequency for both polarizations simultaneously and that the experimental results do show that such a radome can be designed by the procedures used.

7. Discrepancies.

It is appropriate that some of the reasons for the discrepancies noted in the comparison of experimental results with theory be considered. They may be grouped into two major divisions:

FIG. 13

A COMPARISON OF RADOME REFLECTION COEFFICIENTS vs. ANGLE OF INCIDENCE FOR PERPENDICULAR POLARIZATION.

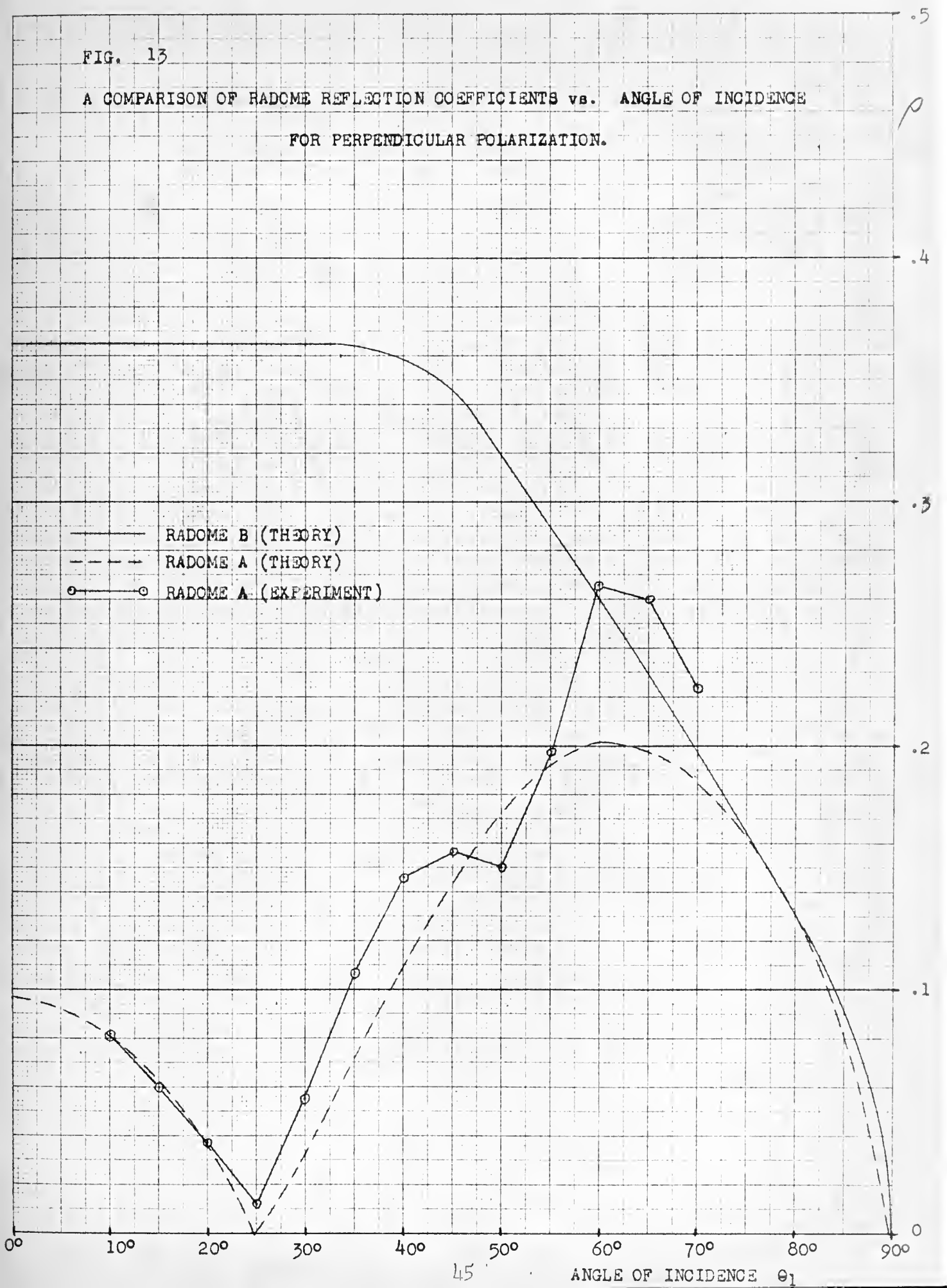

FIG. 14

A COMPARISON OF RADOME REFLECTION COEFFICIENTS vs. ANGLE OF INCIDENCE FOR PARALLEL POLARIZATION.

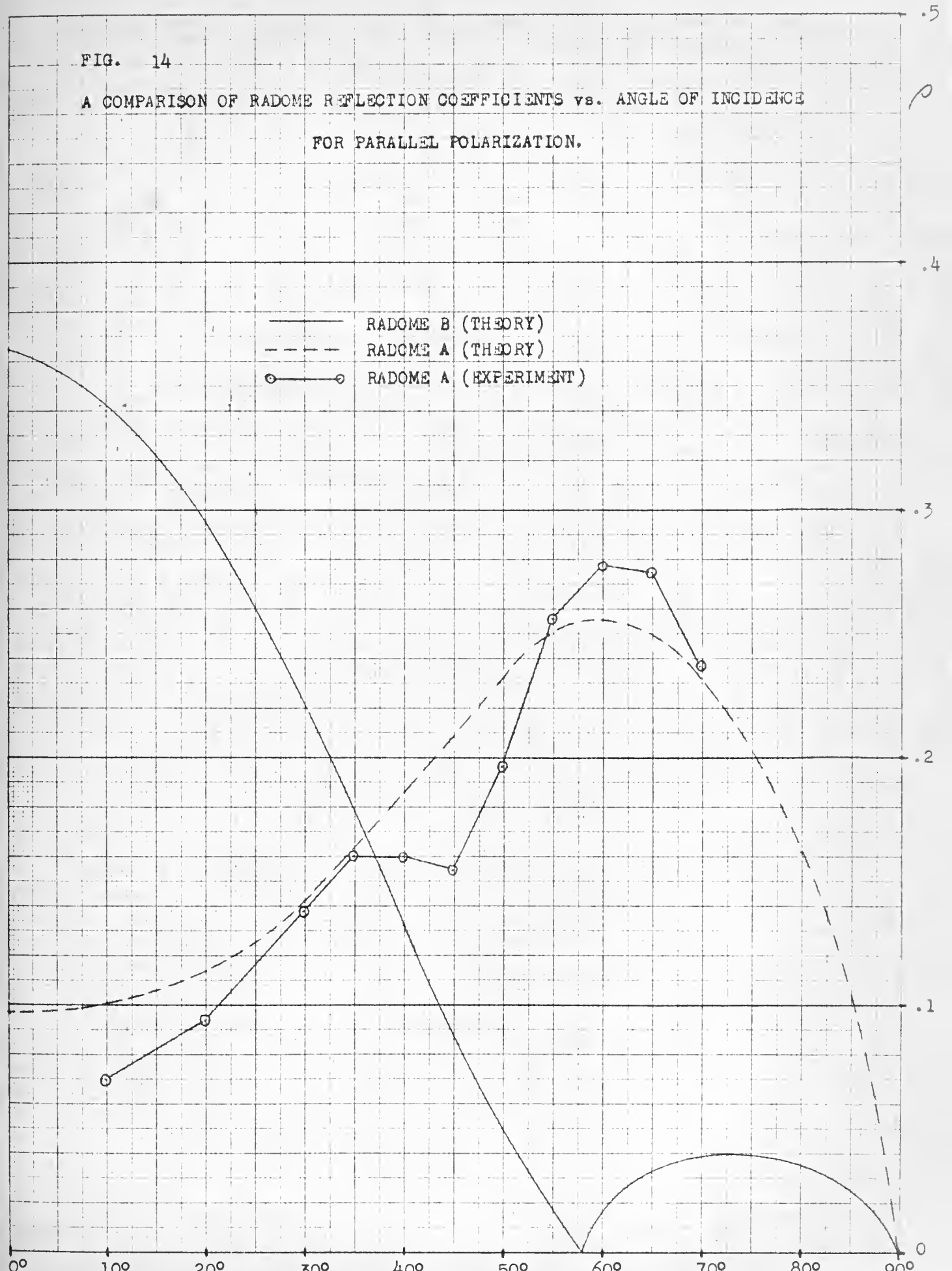

a. Experiment and construction inaccuracies -- Design calculations were carried to four decimal places and a tolerance of plus or minus .001 inch was specified in the construction diagrams. However, the machining of the dielectric plastic to a flat surface is almost impossible. The material, even though it is held flat during the cutting process, will invariably warp as soon as it is released. As a result, the .001 inch tolerance was not maintained.

The testing procedure was the source of most of the errors. It is difficult to obtain accurate results with microwave measurements unless the tests are performed in a closed system. The following reasons are among the most probable causes of experimental errors:

The effects of the standing waves were not completely averaged out.

The power reflected from the standard may not have been the value predicted.

The cancellation network was not completely effective.

b. Theoretical approximations -- As in many involved problems, many approximations are made in order to render the theory less complicated. Such simplifications are valid provided the errors introduced by their use are sufficiently small. Some of the theoretical approximations made are listed here for reference:

The mutual effect of the stored fields around the two wire grids was neglected.

The finite length of the wires was considered infinite.

The susceptance of the wire grids were calculated, in part, from the equations for grids of thin strips.

CHAPTER V

FUTURE POSSIBILITIES

1. Designs of Tomorrow.

With the ever increasing speed of aircraft goes the need of higher strength and higher temperature resistant materials. Radomes that satisfactorily suited yesterday's needs would break up or melt if employed on tomorrow's planes. With the increased speed is the need for more streamlined airframes and more accurate radar systems. The guidance and control of high speed guided missiles must not be overlooked either.

Heavy, pointed radomes made of high temperature resistant ceramic materials, both electrically and structurally enhanced by the inclusion of embedded wires, can be seen as a possible solution. Narrow-band designs using embedded reactive walls may be utilized for isolation of control and interference elimination. Mass produced radomes effective over a broad frequency range and thus suited for use with different radars may have economic and logistic advantages. The anti-icing possibilities of a radome with wires embedded in it are manifest. Without a doubt, reactive walls will be used in future designs, making possible radomes of unusual characteristics.

2. Opportunities for Further Investigation.

The work described in this paper evolved from the question, "Can a design procedure be developed which will allow the construction of a broad-angle radome by the inclusion of reactive walls?" It has been shown that the answer is affirmative. Furthermore, an illustrative design and construction has been provided to demonstrate the procedure

developed, and experimental tests have been conducted to validate the theory. Although this thesis is part of a larger project, it is complete within itself. A question has been posed, and it has been answered. Nevertheless, opportunities for further investigation are evident.

An investigation of low reflection properties alone does not completely describe a radome. For instance -- in many fire-control applications, a linear relation between insertion phase shift and angle of incidence is desired. This problem, in respect to the loaded broad-angle radome, has been considered only in a cursory manner. The results of this superficial investigation were considered satisfactory, but not ideal. Here, obviously, is an opportunity for further endeavor.

Other opportunities develop as one considers the use of different materials and frequencies as well as different placement and number of embedded walls. Questions still unanswered are: How well will a broad-angle radome with embedded wire grids perform at frequencies other than the design frequency? Can a satisfactory broad-angle, and simultaneously broad-band, radome be designed by including reactive walls in its construction? How easily can the loaded radome be mass produced?

BIBLIOGRAPHY

1. Cady, Karelitz and Turner — RADAR SCANNERS AND RADOMES, Part II MIT Radiation Laboratory Series No. 26 McGraw-Hill, 1948

2. Honey, R. C., et. al. — INVESTIGATION OF WIDE-BAND ANTENNAS ABOVE 2000 MC, First Annual Report Contract No. DA-36-039 SC-63236 Chapter VIII, Stanford Research Institute, Menlo Park, Calif., 1955

3. Honey, R. C., et. al. — INVESTIGATION OF WIDE-BAND ANTENNAS ABOVE 2000 MC, Fifth Quarterly Report Contract No. DA-36-039 SC-63236, Chapter VI, Stanford Research Institute, Menlo Park, Calif., 1955

4. Smith, P. H. — TRANSMISSION LINE CALCULATOR Electronics, January, 1939, and January, 1944

5. Ramo and Whinnery — FIELDS AND WAVES IN MODERN RADIO Wiley, 1953

6. Jordan, E. C. — ELECTROMAGNETIC WAVES AND RADIATING SYSTEMS, p 138 Prentice-Hall, 1950

7. MacFarlane, G. G. — SURFACE IMPEDANCE OF AN INFINITE PARALLEL WIRE GRID AT OBLIQUE ANGLES OF INCIDENCE J. I. E. E. (London), 93, Part IIIA pp 1523-1527, 1947

8. Jordan, E. C. — ELECTROMAGNETIC WAVES AND RADIATING SYSTEMS, p 583 Prentice-Hall, 1950

9. Marcuvitz, N. — WAVEGUIDE HANDBOOK McGraw-Hill, 1951

10. Von Hippel, A R. — DIELECTRIC MATERIALS AND APPLICATIONS M.I.T. & Wiley, 1954

11. Redheffer, R. M — THE INTERACTION OF MICROWAVE ANTENNAS WITH DIELECTRIC SHEETS, Radiation Laboratory Report #483/18, March 1, 1946

ADDITIONAL REFERENCE

Horton, M. C., et. al. — OPTICAL THEORY FOR MICROWAVE TRANSMISSION THROUGH DIELECTRIC WALL STRUCTURES
Paper presented at URSI meeting on Microwave Optics, McGill University, June, 1953

Mathis, H. F. — TRANSMISSION CHARACTERISITCS OF SANDWICHES
Correspondence, IRE Transactions on Microwave Theory and Techniques, p 57, October, 1955

Montgomery, C. G. — TECHNIQUE OF MICROWAVE MEASUREMENTS
M.I.T. Radiation Lab. Series, No. 11
McGraw-Hill, 1947

Montgomery, Dicke and Purcell — PRINCIPLES OF MICROWAVE CIRCUITS
M.I.T. Radiation Lab. Series, No. 8
McGraw-Hill, 1948

Oleesky, S. S. — DESIGNING RADOMES FOR SUPERSONIC SPEEDS
Electronics, January, 1954, p 130

Oleesky, S. S. — DEVELOPMENT OF A HIGH-TEMPERATURE MISSILE RADOME
U. S. Naval Air Development Center Report ADC-EL-10-51

Oleesky, S. S. — THE EFFECT OF ELEVATED TEMPERATURE ON TRANSMISSION OF MICROWAVE ENERGY THROUGH DIELECTRIC SHEETS
U. S. Naval Air Development Center Report ADC-EL-148-49

Oleesky, S. S. — A STUDY OF THE PROBLEM OF ANTI-ICING FOR RADOMES AND ITS POSSIBLE SOLUTIONS
U. S. Naval Air Development Report ADC-EL-86-50

Redheffer, R. M. — ELECTRICAL PROPERTIES OF DOUBLE WALL SANDWICH RADOMES.
Radiation Lab. Report 483-11, February, 1945

ADDITIONAL REFERENCES

Redheffer, R. M.	RADOMES AND SYSTEMS PERFORMANCE Radiation Lab Report 483-6, November 17, 1944
Redheffer, R. M.	TRANSMISSION AND REFLECTION OF PARALLEL PLANE SHEETS Radiation Lab Report 483-12, January 26, 1945
Redheffer, R. M.	TRANSMISSION AND REFLECTION OF SINGLE PLANE SHEETS Radiation Lab. Report 483-4, July 12, 1944
Silver, S.	MICROWAVE ANTENNA THEORY AND DESIGN M.I.T. Radiation Lab. Series No. 12 McGraw-Hill, 1949
Storer, J. E., et. al.	A SIMPLE GRAPHICAL ANALYSIS OF A TWO-PORT WAVEGUIDE JUNCTION Proc. IRE August, 1953 p 1004
Tai, C. T.	ELECTROMAGNETIC BACK-SCATTERING FROM CYLINDRICAL WIRES Journal of Applied Physics, August, 1952, Vol 23, No. 8, pp 909-916
Van Vleck, J. H., et. al.	THEORY OF RADAR REFLECTION FROM WIRES OR THIN METALLIC STRIPS Journal of Applied Physics, Vol 18, No. 3, pp 274-294, March, 1947
Wait, J. R.	REFLECTION FROM A WIRE GRID PARALLEL TO A CONDUCTING PLANE Canadian Journal of Physics, September, 1954
Wolin, I.	ELECTRICAL DESIGN OF LOSSY HIGH-INCIDENCE RADOMES U. S. Naval Air Development Center Report ADC-EL-123-50

APPENDIX I

MIDPLANE SOLUTION OF INSERTION LOSS FOR A SYMETRICAL, LOSSLESS, TWO-TERMINAL-PAIR NETWORK[1]

In the following discussion, transmission-line and lumped-constant equivalent circuits will be used. This analogy is also valid for the behavior of infinite dielectric materials in the presence of plane electromagnetic waves.

Consider a system of two, two-terminal-pair, lossless, "half sections" each the mirror image of the other and arranged as illustrated in Figure 15. It will be shown that the voltage standing wave ratio, (the magnitude of the reflection coefficient, the per cent power transmitted, the power insertion loss, etc.), can be easily obtained from only a knowledge of the phase angle of the admittance at the midplane. The analytical proof that this is true will be demonstrated together with a simple graphical procedure. This graphical method proved not only simpler in practice than a laborsome analytical approach, but also presented a representation of the circuit such that the effects of a change of any parameter could be recognized and the ultimate effect evaluated.

Initially consider only one of the two-terminal-pairs, i.e., one half of the system of Figure 15. Let this "half section" be set up for testing as shown in Figure. 16. The voltage reflection coefficient is known to be

[1]Due to S. B. Cohn, Stanford Research Institute.

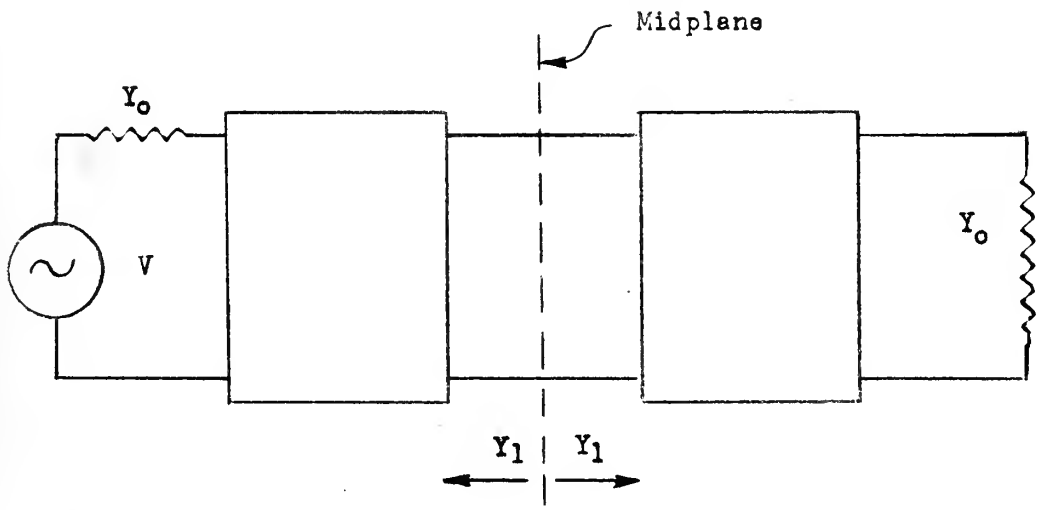

FIG. 15 EQUIVALENT WHOLE SECTION

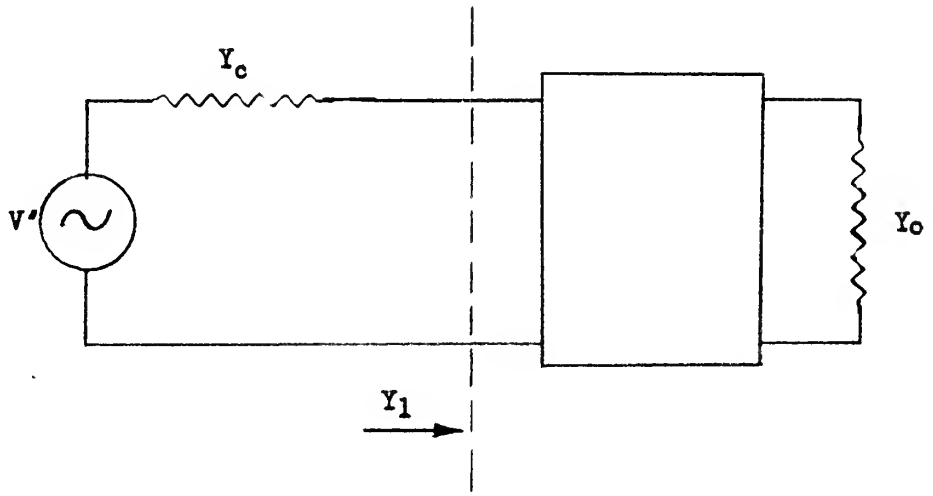

FIG. 16 EQUIVALENT HALF-SECTION

$$\Gamma = \frac{Y_c - Y_1}{Y_c + Y_1} \tag{1}$$

When Y_c is equal to 1

$$\Gamma = \frac{1 - Y_1}{1 + Y_1} \tag{2}$$

Substituting for Y_1, the reflection coefficient becomes

$$\Gamma = \frac{1 - G_1 - j B_1}{1 + G_1 + j B_1} \tag{3}$$

and

$$|\Gamma| \triangleq \rho = \left[\frac{(1-G_1)^2 + B_1^2}{(1+G_1)^2 + B_1^2} \right]^{1/2} \tag{4}$$

Now if the value of Y_c is made different from 1, i.e., the characteristic admittance of the slotted line used for measuring the standing wave ratio of the half section is made different from one, obviously a different standing wave ratio will be measured. Let

$$Y_c = \sqrt{G_1^2 + B_1^2} \tag{5}$$

which is equal to the magnitude of Y_1. This is equivalent to letting Y_c remain equal to one and changing Y_1 so that [1]

$$Y_1 \Rightarrow G^2 + B^2 = 1 \qquad (6)$$

The subscript 1 will now be dropped since Y is no longer truly the midplane admittance. (The ease with which this renormalization is handled by graphical means will be shown shortly.)

Substituting equation (6) into (4)

$$\rho = \left[\frac{1 - 2G + G^2 + B^2}{1 + 2G + G^2 + B^2} \right]^{1/2} = \frac{\sqrt{1-G}}{\sqrt{1+G}} \qquad (7)$$

The voltage standing wave ratio measured in this manner is defined as

$$VSWR_{1/2} = \frac{1+\rho}{1-\rho} \qquad (8)$$

Substituting from (7)

$$VSWR_{1/2} = \frac{\sqrt{1+G} + \sqrt{1-G}}{\sqrt{1+G} - \sqrt{1-G}} = \frac{1+B}{G} = \frac{\sqrt{1+B}}{\sqrt{1-B}} \qquad (9)$$

[1]For example: Let $Y_1 = 4 + j3$ and $Y_c = \sqrt{16 + 9} = 5$. Divide the existing series circuit by 5 so that $Y = 4/5 + j3/5$ and $Y_c = 1$. Now $G^2 + B^2 = \frac{16}{25} + \frac{9}{25} = 1$ Q.E.D. Note that $G/B = G_1/B_1$ which shows that the phase angle has not been changed.

Now consider the entire section shown in Figure 17. Using Thevenin's theorem it can be represented as shown in Figure. 18. As before let

$$G^2 + B^2 = 1 \tag{6}$$

It follows that

$$\Gamma = \frac{G - j2B - G}{G + j2B + G} = \frac{-jB}{G + jB} \tag{10}$$

and

$$|\Gamma| \triangleq \rho = \frac{B}{\sqrt{G^2+B^2}} = B = \frac{1}{\sqrt{1+(G/B)^2}} \tag{11}$$

The voltage standing wave ratio is

$$VSWR = \frac{1+B}{1-B} = \left(VSWR_{1/2}\right)^2 \tag{12}$$

Thus the standing wave ratio for the whole section is the square of the standing wave ratio of the half section, when the half section is measured on the special slotted line of characteristic admittance

$$Y_c = \sqrt{G_1^2 + B_1^2} \tag{5}$$

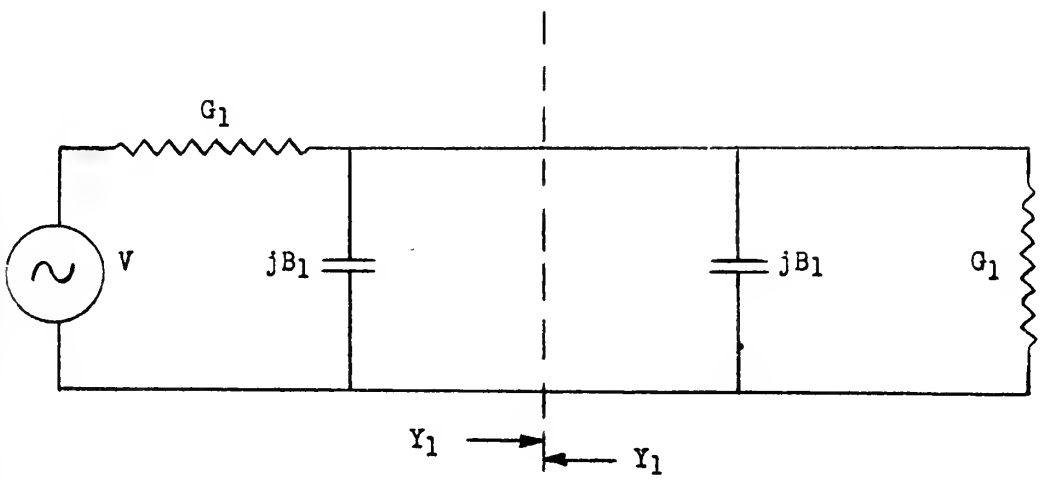

FIG. 17 EQUIVALENT WHOLE SECTION

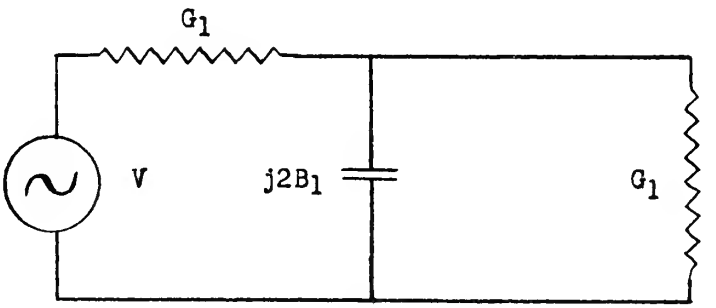

FIG. 18 THEVENIN EQUIVALENT OF WHOLE SECTION

This procedure is accomplished easily on the Smith chart. See Figure 3. After arriving at point "4", which is Y_1/Y_2, proceed on a curve of constant phase angle, i. e., a curve upon which the ratio of G/B does not change. Such a curve is the constant phase angle curve of a Carter or Z-θ chart. (A transparent overlay of such a chart is helpful.) Continue until the line of normalized-admittance-equals-one is reached. This, of course, corresponds to renormalizing Y_1/Y_2 to Y_1/Y_c where the magnitude of Y_1/Y_c equals one. The fraction of the radius on the Smith chart, as measured along the conductance component scale, of the distance from the origin to this point "5", is the value of the standing wave ratio VSWR-1/2. This distance can be easily measured by swinging an arc intercepting the conductance component scale where its values are greater than one. The square of this VSWR-1/2 is the desired standing wave ratio of the entire section.

The construction of points "5" and "6" on Figure 3 can be eliminated by either using a Carter chart transparent overlay and a table relating the phase angle on the chart to the standing wave ratio, or a special overlay can be constructed which is calibrated in standing wave ratio or reflection coefficient.

APPENDIX II

THE REFLECTION COEFFICIENT EQUATION FOR A DIELECTRIC SHEET WITH EMBEDDED INDUCTIVE WALLS

By use of equivalent transmission-line circuit concepts, a dielectric sheet with embedded reactive walls can be represented as shown in Figure 1. Making use of the midplane technique described in Appendix I, only half of this representation is required in order to express the reflection coefficient or standing wave ratio for the entire sheet. This half section with the pertinent parameters appears in Figure 19.

From transmission-line theory, for a lossless dielectric, the input admittance at point "d" is

$$Y_d = Y_2 \left(\frac{(Y_0/Y_2 + j \tan \phi'}{1 + j (Y_0/Y_2) \tan \phi'} \right) \qquad (1)$$

and the input admittances at point "e" and the midplane respectively, become

$$Y_e = j B_w + Y_d = j B_w + Y_2 \left(\frac{(Y_0/Y_2) + j \tan \phi'}{1 + j (Y_0/Y_2) \tan \phi'} \right) \qquad (2)$$

$$Y_1 = Y_2 \left(\frac{(Y_e/Y_2) + j \tan \phi''}{1 + j (Y_e/Y_2) \tan \phi''} \right) \qquad (3)$$

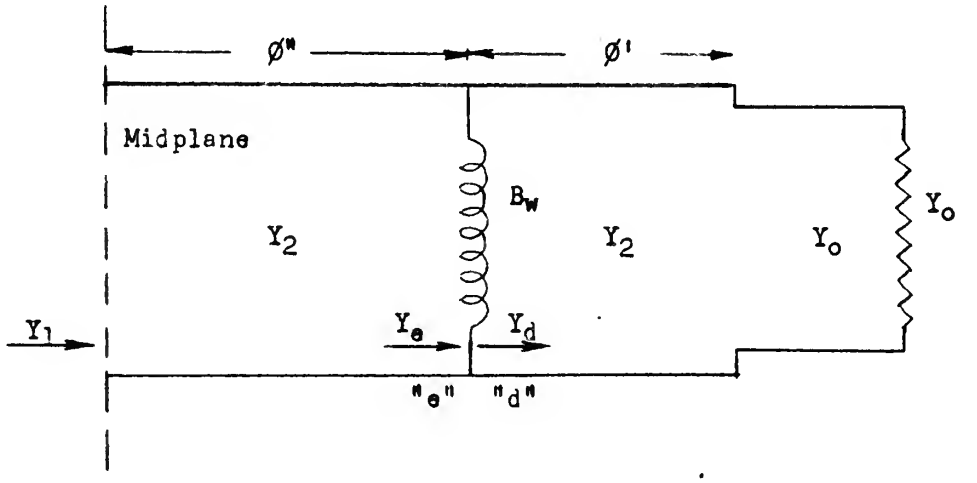

FIG. 19 EQUIVALENT HALF-SECTION OF A LOADED RADOME

A direct substitution of equation (2) into equation (3) and expansion at this point yields a very involved and long expression. Since, by the method of Appendix I, it is sufficient to know the value of G_1/B_1 only, an explicit expression for Y_1 is not needed.

It is convenient to normalize to the characteristic admittance of the dielectric. Separating Y_e/Y_2 into its real and imaginary parts gives

$$Y_e/Y_2 = \frac{G_e}{Y_2} + j\frac{B_e}{Y_2} \tag{4}$$

Where, from equation (2) after rearranging,

$$\frac{G_e}{Y_2} = \frac{Y_0/Y_2\left(1+\tan^2\phi'\right)}{1+\left(Y_0/Y_2\right)^2\tan^2\phi'} \tag{5}$$

and

$$\frac{B_e}{Y_2} = \frac{\left[1-\left(Y_0/Y_2\right)^2\right]\tan\phi' + \frac{B_w}{Y_2}\left[1+\left(Y_0/Y_2\right)\tan^2\phi'\right]}{1+\left(Y_0/Y_2\right)^2\tan^2\phi'} \tag{5a}$$

Now substitute equation (4) into equation (3),

$$\frac{Y_1}{Y_2} = \frac{\frac{G_e}{Y_2} + j\frac{B_e}{Y_2} + j\tan\phi''}{1+j\left(\frac{G_e}{Y_2}+j\frac{B_e}{Y_2}\right)\tan\phi''} \tag{6}$$

Expanding and combining real and imaginary parts, equation (6) becomes

$$\frac{Y_1}{Y_2} = \frac{G_1}{Y_2} + j\frac{B_1}{Y_2} = \frac{\frac{Ge}{Y_2}\left(1+\tan^2\phi''\right)}{\left(1-\frac{Be}{Y_2}\tan\phi''\right)^2+\left(\frac{Ge}{Y_2}\tan\phi''\right)^2} \tag{7}$$

$$+j\left\{\frac{\frac{Be}{Y_2}+\tan\phi''-\left(\frac{Ge}{Y_2}\right)^2\tan\phi''-\left(\frac{Be}{Y_2}\right)^2\tan\phi''-\frac{Be}{Y_2}\tan^2\phi''}{\left(1-\frac{Be}{Y_2}\tan\phi''\right)^2+\left(\frac{Ge}{Y_2}\tan\phi''\right)^2}\right\}$$

It follows that

$$\frac{G_1}{B_1} = \frac{\frac{Ge}{Y_2}\left(1+\tan^2\phi''\right)}{\frac{Be}{Y_2}+\tan\phi''-\left(\frac{Ge}{Y_2}\right)^2\tan\phi''-\left(\frac{Be}{Y_2}\right)^2\tan\phi''-\frac{Be}{Y_2}\tan^2\phi''} \tag{8}$$

In equations (5) and (5a) let the denominators

$$1+\left(Y_0/Y_2\right)^2\tan^2\phi' = \Delta \tag{9}$$

It is now valid to say

$$\frac{Ge}{Y_2} \equiv \frac{Ge'}{\Delta} \tag{10}$$

and

$$\frac{Be}{Y_2} \equiv \frac{Be'}{\Delta} \tag{10a}$$

This substitution makes equation (8) the simple expression

$$\frac{G_1}{B_1} = \frac{G_e'\left(1+\tan^2\phi''\right)}{B_e'\left(1-\tan^2\phi''\right)+\left(\Delta^2-G_e'^2-B_e'^2\right)\frac{\tan\phi''}{\Delta}} \tag{11}$$

where obviously

$$G_e' = Y_0/Y_2\left(1+\tan^2\phi'\right) \tag{12}$$

and

$$B_e' = \left[1-\left(Y_0/Y_2\right)^2\right]\tan\phi' + \frac{B}{Y_2}\Delta \tag{12a}$$

(This arrangement, including the disregard of the trigonometric identity $1 + \tan^2 A = \sec^2 A$, is used because it offers ease of computation with a desk calculator.)

Now it is an easy matter to substitute the numerical value of equation (11) into the expression for the reflection coefficient given in Appendix I, i. e.

$$\rho = \frac{1}{\sqrt{1+\left(G_1/B_1\right)^2}} \tag{13}$$

Often when using a calculator to obtain numerical solutions to equations, one explicit expression is not as desirable as several equations, each explicit for one variable or parameter; the final equation utilizing the numerical solution of the previous. Such is the case here, for it is presumed that all design work has been accomplished by graphical procedure and the solution of the analytical equations is for the compilation of theoretical data and further, that a desk calculator will be employed. The resulting expression is no less valid because of this procedure.

F443 Finley
A broad-angle radome employing reactive walls.

DE1161 10585

F443 Finley
A broad-angle radome employing reactive walls.